

Forschungszentrum Karlsruhe

in der Helmholtz-Gemeinschaft

Wissenschaftliche Berichte

FZKA 6600

**Validation of turbulence models
in the computer code FLUTAN for a free hot sodium jet
in different buoyancy flow regimes**

L. N. Carteciano, G. Grötzbach

Institut für Kern- und Energietechnik
Programm Nukleare Sicherheitsforschung

Forschungszentrum Karlsruhe GmbH, Karlsruhe
2003

Impressum der Print-Ausgabe:

**Als Manuskript gedruckt
Für diesen Bericht behalten wir uns alle Rechte vor**

**Forschungszentrum Karlsruhe GmbH
Postfach 3640, 76021 Karlsruhe**

**Mitglied der Hermann von Helmholtz-Gemeinschaft
Deutscher Forschungszentren (HGF)**

ISSN 0947-8620

Validation of turbulence models in the computer code FLUTAN for a free hot sodium jet in different buoyancy flow regimes

ABSTRACT

The large diffusivity for heat and the small one for momentum in general hinder to use the Reynolds analogy to model turbulent heat transfer in liquid metal flows. Nevertheless, most code applications for technical flows are using a turbulent Prandtl number concept for calculating the turbulent heat transfer for any fluid. More adequate for fluids with strongly different diffusivities is to use a full second order modeling. Here, we apply the Turbulence Model For Buoyant Flows (TMBF) and a standard $k-\varepsilon-\sigma_t$ model to recalculate the TEFLU experiments with a free hot sodium jet in several buoyancy regimes. The TMBF is a combination of a standard $k-\varepsilon$ model for the turbulent momentum transfer and a full second order modeling for the turbulent heat fluxes. The numerical results show that the $k-\varepsilon-\sigma_t$ model requires flow dependent local adaptations of the turbulent Prandtl number σ_t for accurate predictions of temperature distributions. In contrast, the TMBF, which has special model extensions for liquid metal flows, achieves widely acceptable results. Possibilities for required further model improvements are discussed.

Validierung der Turbulenzmodelle im Rechenprogramm FLUTAN für einen heißen Natriumfreistrahls bei unterschiedlichen Auftriebsbedingungen

ZUSAMMENFASSUNG

Die Reynolds-Analogie zwischen dem turbulenten Wärme- und dem Impulstransport kann nicht für die Modellierung des turbulenten Wärmetransports in Strömungen mit flüssigen Metallen verwendet werden, da die Diffusivität der Wärme viel größer als die des Impulses ist, und da deshalb auch die turbulenten Geschwindigkeitsfluktuationen und Temperaturfluktuationen nicht ähnlich sind. Trotzdem benutzen die meisten thermohydraulischen Rechenprogramme das Konzept der turbulenten Prandtl-Zahl zur Berechnung des turbulenten Wärmetransports für beliebige Fluide. Bei Fluiden mit stark unterschiedlichen Diffusivitäten sind die Turbulenzmodelle zweiter Ordnung, wie z. B. das im Rechenprogramm FLUTAN implementierte Turbulenzmodell für Auftriebsströmungen (TMBF), geeigneter. Das TMBF ist eine Kombination eines Modells erster Ordnung, nämlich des k - ϵ Modells, für den turbulenten Impulstransport und eines Modells zweiter Ordnung mit fünf Gleichungen für den turbulenten Wärmetransport. Im Rahmen der Validierung von Turbulenzmodellen für flüssige Metalle werden das TMBF und das k - ϵ - σ_t Modell angewendet. Dazu werden die TEFLU-Experimente mit einem beheizten turbulenten Freistrahls in Natrium mit unterschiedlich starken Auftriebseinflüssen nachgerechnet. Die numerischen Ergebnisse zeigen, dass das k - ϵ - σ_t Modell von der Strömung abhängige lokale Anpassungen der turbulenten Prandtl Zahl braucht, um die Temperaturfelder richtig zu berechnen. Dagegen erreicht das TMBF, das eine Modellerweiterung für flüssige Metalle besitzt, überwiegend gute Ergebnisse. Möglichkeiten für weitere notwendige Modellverbesserungen werden diskutiert.

Preface

This analysis is based on the FZK contribution to the common EC project ASCHLIM in which within 2002 an Assessment of Computational Fluid Dynamics codes for Heavy Liquid Metals was performed, contract Nr. FIKW-CT-2001-80121. The computations were done earlier when both authors were members of the Institute of Reactor Safety at Forschungszentrum Karlsruhe. Meanwhile L.N.C. left to SAP Walldorf (D) and Cannes (F), and G.G. moved to the Institut für Kern- und Energietechnik. We would like to thank our former colleagues in the FLUTAN team for their valuable contributions to the development of and analysis with this code; sincere thanks go especially to B. Dorr who already retired, to Dr. X. Jin, and last but not least to W. Olbrich.

List of Contents

List of Contents	1
1 Introduction	1
2 FLUTAN Computer Code	3
3 Turbulence Model for Buoyant Flows TMBF	4
3.1 <i>Turbulent Shear Stress Modeling</i>	4
3.2 <i>Turbulent Heat Flux Modeling</i>	6
3.3 <i>Model Coefficients</i>	8
4 The k-ϵ-σ_t Model	9
5 TEFLU Experiments	10
6 FLUTAN Calculations	12
6.1 <i>Numerical Model Specifications</i>	12
6.1.1 Geometry and Boundary Conditions	12
6.1.2 Physical and Numerical modeling	13
6.2 <i>Results</i>	14
6.2.1 Forced Jet	14
6.2.2 Buoyant Jet	14
6.2.3 Plume	15
7 Discussion	15
8 Conclusions	17
References	19
Figures	24
Tables	32

1 Introduction

In the framework of the Benchmark Working Group (BWG) for Accelerated Driven Systems (ADS) both, experimental and computational investigations are being performed to explore the capability of Computational Fluid Dynamics (CFD) codes to predict heavy liquid metal turbulent flows with heat transfer (Knebel et al. 2000).

The conservation equations for mass, momentum, and thermal energy do not form a closed set of equations if the statistical approach is used to describe turbulence. In fact, unknown correlations called turbulent shear stresses $\overline{U_i'U_j'}$ and turbulent heat fluxes $\overline{U_i'T'}$ exist in these equations. They represent the turbulent transport of momentum and heat. A way of determining these correlations is to adopt turbulence models which introduce laws to simulate the turbulent transport.

A well-known and widely used class of turbulence models is based on the eddy viscosity / eddy heat diffusivity concept (Rodi 1980). The eddy viscosity ν_t and eddy heat diffusivity Γ_t are respectively introduced by a mean gradient approach in the terms representing the turbulent transport of momentum and heat. The eddy viscosity for the turbulent momentum transport is usually approximated by using any variant of the widely known k- ϵ model. The eddy heat diffusivity is approximated mostly much less sophisticated; it is assumed to be also isotropic and to be linked to the eddy viscosity by a fixed turbulent Prandtl number $\sigma_t = \nu_t / \Gamma_t$. This implies that the turbulent transport of heat is assumed to be strictly analogous to the turbulent momentum transport. These assumptions are the basis of the Reynolds analogy. This analogy works well for a wide class of flows but not for liquid metal flows, see Table 1. Due to the strongly different values of relatively small molecular viscosity ν and relatively large thermal diffusivity Γ , the statistical features of the turbulent velocity and temperature fields are not similar. This means, the Reynolds analogy should not be applied because it has no basis for fluids with small molecular Prandtl numbers $Pr = \nu / \Gamma$. For these fluids the turbulent Prandtl number is no longer a fixed value, but it depends on a number of parameters, see e.g. in Kays (1994).

In contrast to this modelling, formulations independent of ν_t should be used to approximate the turbulent eddy conductivity Γ_t in liquid metals, like in the first order 4-equation model by Nagano et al. (1994). Such 4-equation models based not only on k- and ϵ -equations, but in addition on transport equations for the temperature variance and its dissipation or destruction, allow also for different time scales in the turbulent velocity and temperature fields.

For buoyant flows one gets strong anisotropy in the turbulence field due to the orientation of the buoyancy force. In such flows even a second-order description of the turbulent transport of heat should be applied, which means the use of independent transport equations for the three turbulent heat fluxes. Such models are not constrained by any of the above mentioned problems. Therefore, in order to simulate turbulent flows in liquid metals with buoyancy it is reasonable to use a second-order model at least for the turbulent transport of heat.

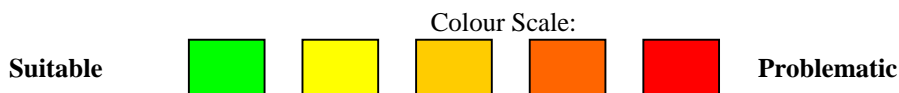
The Turbulence Model for Buoyant Flows (TMBF) (Carteciano 1996) developed and implemented in the CFD Code FLUTAN (Willerding & Baumann 1996) is potentially suitable for the simulation of the turbulent transport of mass, momentum, and heat in liquid metals because it uses a second order model for the turbulent transport of heat,

Table 1. This model was already successfully validated for a sodium flow in a forced convection regime (Carteciano et al. 1997, Baumann et al. 1997). In order to extend the range of the TMBF to low Peclet numbers, new model relationships were introduced into the model based on analyses of direct numerical turbulence simulations (Carteciano et al. 1999); they were previously validated for natural convection by investigating the buoyant air flow along a vertical heated wall (Prudhomme 1998).

This extended version of the TMBF is being validated here for liquid metal flows by means of numerical calculations of a turbulent hot jet in sodium. Unfortunately, there are no sufficiently accurate experimental turbulent heat transfer data available for a heavy liquid metal, so that existing data for the light weight sodium with a smaller Prandtl number were used instead. Using a free jet experiment in a highly turbulent multi-jet surrounding to analyze the performance of turbulence models has the advantage that the numerical results are mainly governed by the turbulence models and do not suffer from any inadequate wall modeling. The experiments were performed in the test facility TEFLU at the Forschungszentrum Karlsruhe (Knebel et al. 1998). Three different buoyancy regimes were considered for the verification of the TMBF which were classified by the experimenters as forced jet, buoyant jet, and plume. The FLUTAN calculations were carried out using not only the TMBF but also the standard $k-\varepsilon-\sigma_t$ model in order to show the advantage of the TMBF compared to the $k-\varepsilon-\sigma_t$ model and to show the limits of applicability of an eddy diffusivity approach to liquid metal flows. In this report, the results, which are compared with experimental data, are documented and discussed.

Table 1: Classification of existing turbulence models for buoyant liquid metal flows.

MODELS	ASSUMPTIONS FOR TURBULENT HEAT TRANSPORT			ASSUMPTIONS FOR TURB. MOMENTUM TRANSPORT		NUMERICAL EFFICIENCY AND ROBUSTNESS
	Reynolds-Analogy	Fourier-Assump.	Isotropic turbulent transport	Boussin.-Assumption	Isotropic turbulent transport	
$k-\varepsilon-\sigma_t$						
$k-\varepsilon-T'^2-\varepsilon_T$						
TMBF						
Algebraic						
Reynolds-Stress						



2 FLUTAN Computer Code

FLUTAN is a highly vectorized computer code for 3d fluid-dynamic and thermal-hydraulic analyses in Cartesian or cylinder coordinates (Willerdig & Baumann 1996). Starting from its methodological precursor COMMIX-2 (Bottoni et al. 1985 and Bottoni & Willerdig 1987) and its highly vectorized and optimized version COMMIX-2(V) (Borgwaldt 1990), FLUTAN was developed in order to simulate single phase flows of several fluids with small compressibility.

The conservation equations for mass, momentum, energy, and the transport equations for the turbulence quantities are discretized on a structured grid by a finite volume method. A staggered grid is used for the velocities. The discretization of the diffusive terms is performed by a central difference scheme. A first order upwind or one of two second order upwind methods can be chosen for the convective terms; i.e. QUICK (Leonard 1979) and LECUSSO (Günther 1992). Several Poisson solvers are available for pressure calculation, e.g. the highly vectorized CRESOR solver (Borgwaldt 1990). A first order implicit Euler-method is used for time discretization.

Recently developed and implemented numerical features are achieving a larger numerical efficiency and an improved numerical accuracy: One is a method to decouple the time integration between the different transport and conservation equations, so that different time steps may be used in the different equations (Moser 1996). An other one is an explicitly treated static local grid refinement method for the Cartesian grid (Ammann 1997). The recent one is a newly developed method to use body fitted coordinates in a code based on a staggered grid: the conservation equations are transformed from the Cartesian to a general curvilinear system by keeping the physical Cartesian velocity components as dependent variables and by defining three Cartesian velocity components on every cell surface (Jin 2001).

Several turbulence models are available in FLUTAN like the Prandtl-mixing length model and models based on transport equations for some turbulence quantities. The most important one is the Turbulence Model for Buoyant Flows (TMBF) which consists of a first order k - ϵ model in a low-Reynolds number formulation and a second order five-equations turbulent heat flux model (Carteciano et al. 1997). In several benchmarks it turned out that the TMBF in its current development status is a powerful tool at least for forced and mixed convection even for liquid metal flows (Baumann et al. 1997).

Special thermal boundary conditions are available in FLUTAN like a heat exchanger model, a one-dimensional wall model, and a model for heat radiation between solid surfaces (Cheng & Müller 1998). A three-dimensional heat conduction model for the structures was developed for the investigation of the SUCOS experiments (Grötzbach et al. 2002a). This is necessary for simulating solid structures with internal non-uniform transport of heat. The structure temperatures are discretized on an own grid on which the heat conduction equation is solved in all dimensions independent of the solution of the corresponding equation in the fluid domain. Accurate coupling of the radiation model and of the 3d structure model to the energy in the fluid is automatically achieved by implementing both models within the outer iteration loop.

For handling of the code a modern graphical user interface was developed in which the programs for pre- and post-processing, for solving the equations, for data conversion, and for maintenance of the FLUTAN code system were implemented. This user interface,

as well as the ONLIVIS program for the local online visualization of some selected results from an ongoing FLUTAN calculation running on an other remote computer system is based on the program language Tcl/Tk; thus, it can be used on Windows and on UNIX-based systems (Carteciano et al. 2001, Olbrich 2001).

3 Turbulence Model for Buoyant Flows TMBF

The TMBF is a combination of a first-order 2-equation model for the turbulent transport of momentum and of a second-order 5-equation model for the turbulent transport of heat. The turbulent stresses are calculated assuming an isotropic eddy viscosity and solving the transport equations for turbulent kinetic energy k and for its dissipation rate ε . The three turbulent heat fluxes $\overline{U_i' T'}$ are determined by means of transport equations for these quantities. Moreover, transport equations for the variance of temperature fluctuations $\overline{T'^2}$ and its dissipation rate ε_T are used in the description of the turbulent transport of heat. All five equations are formulated in a so-called 'low-Peclet number' formulation which means, the conductive wall layers have to be resolved by the grids.

3.1 Turbulent Shear Stress Modeling

The turbulent shear stresses are modeled in the TMBF using the gradient assumption of Boussinesque:

$$-\overline{U_i' U_j'} = \nu_t \left(\frac{\partial \overline{U_i}}{\partial x_j} + \frac{\partial \overline{U_j}}{\partial x_i} \right) - \frac{2}{3} k \delta_{ij}. \quad (1)$$

The isotropic eddy viscosity ν_t is introduced by this assumption. The distribution of ν_t is calculated using an extended Prandtl-Kolmogorov relationship:

$$\nu_t = c_\mu f_\mu \frac{k^2}{\varepsilon}. \quad (2)$$

This relationship contains an empirical coefficient c_μ and a damping function f_μ , which is necessary to extend the validity of this relationship to low Reynolds numbers $Re_\tau = U_\tau y / \nu$ ($U_\tau =$ shear velocity). In this model, the formulation for f_μ which was proposed by Nagano and Kim (1988) is used for smooth walls:

$$f_\mu = [1 - \exp(-Re_\tau / 26.5)]^2. \quad (3)$$

In order to calculate the eddy viscosity, the transport equations of the turbulent kinetic energy k and its dissipation rate ε are solved:

$$\frac{\partial k}{\partial t} + \overline{U}_i \frac{\partial k}{\partial x_i} = \frac{\partial}{\partial x_i} \left[\left(\frac{v_t}{\sigma_k} + \nu \right) \frac{\partial k}{\partial x_i} \right] + P_k + G_k - \varepsilon - 2\nu \left(\frac{\partial \sqrt{k}}{\partial x_i} \right)^2, \quad (4)$$

$$\frac{\partial \varepsilon}{\partial t} + \overline{U}_i \frac{\partial \varepsilon}{\partial x_i} = \frac{\partial}{\partial x_i} \left[\left(\frac{v_t}{\sigma_\varepsilon} + \nu \right) \frac{\partial \varepsilon}{\partial x_i} \right] + P_{\varepsilon b} - S_\varepsilon + \nu v_t (1 - f_\mu) \left(\frac{\partial^2 \overline{U}_i}{\partial x_j \partial x_i} \right)^2, \quad (5)$$

$$P_k = \nu_t \left(\frac{\partial \overline{U}_i}{\partial x_j} + \frac{\partial \overline{U}_j}{\partial x_i} \right) \frac{\partial \overline{U}_i}{\partial x_j}, \quad (6)$$

$$G_k = -\beta g_i \overline{U}_i' T', \quad (7)$$

$$P_{\varepsilon b} = \frac{\varepsilon}{k} c_{\varepsilon 1} (P_k + G_k) (1 + c_{\varepsilon 3} Ri_f), \quad (8)$$

$$S_\varepsilon = \frac{\varepsilon^2}{k} f_2 c_{\varepsilon 2}, \quad (9)$$

$$f_2 = 1 - 0.3 \exp \left(-Re_t^2 \right). \quad (10)$$

The turbulent diffusion terms of the transport equations for k and ε are modeled with mean gradient assumptions (Rodi 1972). In order to consider the buoyancy influence on ε , the production term $P_{\varepsilon b}$ contains the buoyancy term G_k and a correction term depending on the flux Richardson number Ri_f (eq. 8). This number is defined as

$$Ri_f = -0.5 G_V / (P_k + G_k)$$

where G_V is the buoyancy production of only the lateral energy component V' (Rodi 1980). For the sink term S_ε in the transport equation for ε , the modeling of Jones & Launder (1972) is used (eq. 9 and eq. 10) with a correction function f_2 for the empirical coefficient $c_{\varepsilon 2}$ in order to extend the validity of the standard value of $c_{\varepsilon 2}$ to locally low turbulence Reynolds numbers:

$$Re_t = k^2 / (\nu \varepsilon)$$

The transport equations for k and ε contain the buoyancy term G_k which depends on the turbulent heat fluxes (eq. 7). This is an important term for a turbulence model for buoyant flows because it represents the only mechanism in which the temperature field affects the turbulence in the momentum field by means of buoyancy.

3.2 Turbulent Heat Flux Modeling

The TMBF does not apply first order turbulent heat flux modeling by introducing gradient assumptions and eddy conductivities, but it solves the second order transport equations for the turbulent heat fluxes; therefore, it incorporates a detailed modeling of G_k . The modeled transport equations for the three turbulent heat fluxes are as follows (for $i=1,2,3$):

$$\frac{\partial \overline{U'_i T'}}{\partial t} + \overline{U'_j} \frac{\partial \overline{U'_i T'}}{\partial x_j} = \frac{\partial}{\partial x_j} \left(\left[c_{TD} \frac{k^2}{\varepsilon} + \frac{\Gamma + \nu}{2} \right] \frac{\partial \overline{U'_i T'}}{\partial x_j} \right) - \left(\overline{U'_i U'_j} \frac{\partial \overline{T}}{\partial x_j} + \overline{U'_j T'} \frac{\partial \overline{U}_i}{\partial x_j} \right) - G_{U'_i T'} + \pi_i + \varepsilon_{U T'} \quad (11)$$

The molecular and turbulent diffusion terms are modeled by mean gradient assumptions (Launder 1978). The modeling of the pressure-temperature gradient correlation π_i of Monin (1965) and Launder (1975) also contains a wall function in order to consider the damping effect of the wall on the turbulent heat flux perpendicular to the wall (Gibson & Launder 1978):

$$\pi_i = -c_{T1} \frac{\varepsilon}{k} \overline{U'_i T'} + c_{T2} \overline{U'_j T'} \frac{\partial \overline{U}_i}{\partial x_j} + c_{T3} \beta g_i \overline{T'^2} - c_{T4} \frac{\varepsilon}{k} \overline{U'_{[n]} T'} \delta_{i[n]} \frac{k^{3/2}}{x_{[n]} \varepsilon} \quad (12)$$

There is no summation over the index n , which indicates the normal direction to a wall.

The modeling of the dissipation or destruction rate of the heat fluxes $\varepsilon_{U T'}$ is based on ideas of Shikazono & Kasagi (1990) with an additional term for liquid metal heat transfer:

$$\varepsilon_{U T'} = -\frac{1 + \text{Pr}}{2\sqrt{\text{Pr}}\sqrt{R}} \left(\frac{\varepsilon}{k} \right) \exp \left[-c_{T5} (\text{Re}_t + \text{Pe}_t) \right] \overline{U'_i T'} \quad (13)$$

The contribution of this term in the transport equation (11) is negligible at high Peclet numbers but becomes important at low Peclet numbers. For this reason, an exponential function of not only the turbulence Reynolds number, but of the sum of the local turbulence Reynolds and Peclet numbers ($\text{Pe}_t = \text{Re}_t * \text{Pr}$) is introduced here, which is supported by the Direct Numerical Simulation (DNS) investigations of Wörner & Grötzbach (1995). The complete expression of this modeling can be derived by dimensional analysis (Carteciano 1996).

The transport equation (11) contains a buoyancy term $G_{U'_i T'}$ in which the variance of the temperature fluctuations $\overline{T'^2}$ appears formally:

$$G_{U'_i T'} = \beta g_i \overline{T'^2} \quad (14)$$

Thus, for a detailed description of buoyancy effects, a transport equation for the variance of the temperature fluctuations $\overline{T'^2}$ is also solved:

$$\frac{\partial \overline{T'^2}}{\partial t} + \overline{U}_i \frac{\partial \overline{T'^2}}{\partial x_i} = \frac{\partial}{\partial x_i} \left[\left(c_{TT} \frac{k^2}{\varepsilon} + \Gamma \right) \frac{\partial \overline{T'^2}}{\partial x_i} \right] - 2 \overline{U'_i T'} \frac{\partial \overline{T}}{\partial x_i} - 2 \varepsilon_{T'} - 2 \Gamma \left(\frac{\partial \sqrt{\overline{T'^2}}}{\partial x_i} \right)^2. \quad (15)$$

This equation contains the modeling of Spalding (1971) for the turbulent diffusion term and the modeling of Nagano & Kim (1988) to consider the low Peclet number effects.

The dissipation rate of the temperature variance $\varepsilon_{T'}$ is often modeled using the definition of the turbulent time-scale ratio R:

$$\varepsilon_{T'} = \frac{\overline{\varepsilon T'^2}}{2 R k}. \quad (16)$$

In this modeling, R is usually assumed to be constant. This assumption is not satisfactory because from our current understanding of the spectral distribution of the quantities appearing in eq. (16) we have to expect that R depends on the Reynolds number, on the type of the flow, on the molecular Prandtl number, on wall distance, and even on the type of thermal boundary conditions. To avoid the problems with the limited knowledge on R for an arbitrary type of flow, a transport equation for $\varepsilon_{T'}$ can optionally be solved in the TMBF instead of using eq. (16):

$$\begin{aligned} \frac{\partial \varepsilon_{T'}}{\partial t} + \overline{U}_i \frac{\partial \varepsilon_{T'}}{\partial x_i} = \frac{\partial}{\partial x_i} \left(c_{DD} \frac{k^2}{\varepsilon} + \Gamma \right) \frac{\partial \varepsilon_{T'}}{\partial x_i} - \varepsilon_{T'} \left(c_{D1} \frac{\varepsilon_{T'}}{T'^2} + c_{D2} \frac{\varepsilon}{k} + c_{P1} \frac{\overline{U'_i T'}}{T'^2} \frac{\partial \overline{T}}{\partial x_i} - c_{P2} \frac{P_k}{k} \right) \\ + 2 \Gamma \Gamma_i \left(\frac{\partial^2 \overline{T}}{\partial x_i \partial x_j} \right)^2. \end{aligned} \quad (17)$$

The models proposed by Hanjalic (1994) are used in this equation. Furthermore, the modeling of Nagano & Kim (1988) is introduced in order to consider the low Peclet number effects.

In order to extend the range of applicability of the TMBF model to very low Prandtl numbers, new optional model relationships have been implemented in the production-buoyancy term $P_{\varepsilon b}$ (eq. 8) of the ε equation and for the dissipation term $\varepsilon_{U'_i T'}$ (eq. 13) of the turbulent heat flux equations (Carteciano et al. 1999). These were deduced by means of an analytical method using the two-point correlation technique, Ye et al. (1997) and Wörner et al. (1999). The models were calibrated using the DNS data base by Wörner & Grötzbach (1997) for several buoyant flows in fluids with Prandtl numbers ranging from 0.006 to 7. The new optional model extensions, which replace those in equations (8) and (13) are:

$$P_{\varepsilon b} = \frac{\varepsilon}{k} \left(c_{\varepsilon 1} P_k + \left(\frac{\text{Pr}}{R} \right)^{0.7} G_k \right); \quad (18)$$

$$\varepsilon_{U'_i T'} = -\frac{1}{2} \left(1 + \frac{1}{\text{Pr}} \right) \left(\frac{\text{Pr}}{R} \right)^{0.7} \left(\frac{\varepsilon}{k} \right) \overline{U'_i T'}. \quad (19)$$

In this extended turbulent heat flux model with 5 transport equations, the required very problematic time scale ratio R has not to be specified as a model parameter, but it can be calculated from eq. (16), see chapter 7.

The interaction due to buoyancy between the transport equations for turbulence quantities is complex in this TMBF model. This interaction is roughly represented in Fig. 1. An important feature which gets obvious from this figure is, that the turbulent heat fluxes in buoyant flows may become strongly anisotropic due to source terms containing temperature variances. On the other hand, the turbulent heat fluxes themselves are the important buoyant source or sink terms in the k and ε equations. Having in both terms results of modeled transport equations instead of using algebraic model relations is an advantage regarding an adequate phenomenological behavior and also regarding the accuracy of the TMBF.

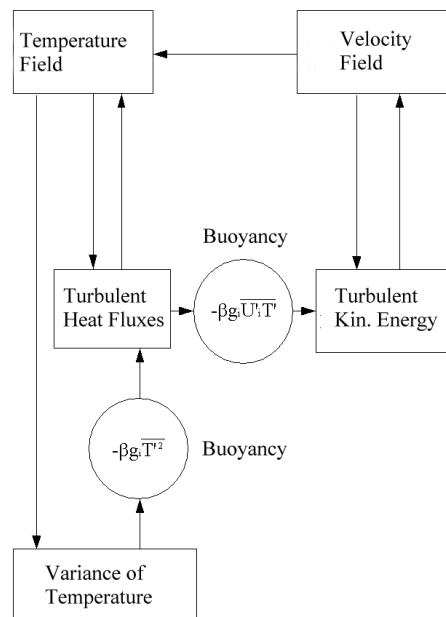


Fig. 1: Coupling between turbulence quantities in the TMBF.

3.3 Model Coefficients

The extended TMBF contains seven transport equations and 17 empirical coefficients. The standard set of empirical coefficients (Table 2) from Gibson & Launder (1978) and Nagano & Kim (1988) is used in the TMBF. The model has been implemented in the FLUTAN computer code and it has been validated by means of experimental data from turbulent flows in forced, mixed and natural convection; examples are given in (Carteciano et al. 1997, 1999, and Prudhomme 1998).

The TMBF does not introduce six additional transport equations for the turbulent shear stresses and thus differs from a so-called full Reynolds stress model. However, the calculated turbulent stresses and heat fluxes are no longer related through a fixed turbulent Prandtl number and are therefore not linked by the Reynolds analogy. In contrast, due to

the separate modeling it is possible to analyze an approximate spatial distribution for the turbulent Prandtl number σ_t from the numerical results, see chapter 7.

Table 2: Standard set of empirical coefficients in the TMBF.

k-tr.eq.		ε -tr. eq		$\overline{U'_i T'}$ -tr. eq.		$\overline{T'^2}$ -tr.eq.		$\varepsilon_{T'}$ -tr.eq.	
coeff.	value	coeff.	value	coeff.	value	coeff.	value	coeff.	value
σ_k	1.0	σ_ε	1.3	c_{TD}	0.11	c_{TT}	0.13	c_{DD}	0.13
c_μ	0.09	$c_{\varepsilon 1}$	1.44	c_{T1}	3.0			c_{D1}	2.2
		$c_{\varepsilon 2}$	1.92	c_{T2}	0.33			c_{D2}	0.8
		$c_{\varepsilon 3}$	0.8	c_{T3}	0.5			c_{P1}	1.8
				c_{T4}	0.5			c_{P2}	0.72

4 The k- ε - σ_t Model

In the following calculations of the sodium jet experiments, also the widely used turbulent Prandtl number concept will be applied for comparison. Therefore, this model is also shortly introduced.

The common k- ε - σ_t model is a first-order 2-equation model. It consists of the transport equations of k (eq. 4) and ε (eq. 5) using an isotropic eddy viscosity (eq. 2) and of a simple isotropic heat flux approximation. A constant turbulent Prandtl number σ_t is used to approximate the turbulent thermal conductivity Γ_t from the turbulent viscosity calculated by the k- ε model:

$$\Gamma_t = \frac{\nu_t}{\sigma_t}. \quad (20)$$

This means, the Reynolds analogy is assumed. This is a very crude approximation for liquid metal flows, because the strongly different molecular diffusivities for momentum and heat cause large differences in the thicknesses of the viscous and conductive wall layers. An additional problem may arise from the large differences in the time scales of the turbulent velocity and temperature fluctuations in liquid metals. Instead of solving the transport equations for the turbulent heat fluxes like in the TMBF model (eq. 11), these fluxes are calculated by using the gradient assumption of Fourier:

$$-\overline{U'_i T'} = \Gamma_t \frac{\partial \overline{T}}{\partial x_i}. \quad (21)$$

Different to the TMBF model (eq. 7), in which the buoyancy term G_k needs no model assumptions, here it has to be modeled e.g. by using eq. (20) and eq. (21):

$$G_k = \beta g_i \frac{v_t}{\sigma_t} \frac{\partial \bar{T}}{\partial x_i}. \quad (22)$$

The production term due to buoyancy P_{eb} in the transport equation for ε is modeled like in eq. (8).

The standard set of coefficients of this model is summarized in Table 3. For the turbulent Prandtl number, the standard value is $\sigma_t = 0.9$.

This model is also implemented in the FLUTAN code. Like the TMBF model, it is available in a low-Reynolds number formulation which requires an adequate resolution of the viscous wall layer; in addition it is available in a simpler high Reynolds number version which, for wall bounded flows,

has to be used together with wall functions for the mean velocity field and at Prandtl numbers greater or around one also for the temperature field.

Table 3: Standard set of empirical coefficients in the k - ε - σ_t model.

k-tr.eq.		ε-tr. eq	
coeff.	value	coeff.	value
σ_k	1.0	σ_ε	1.3
c_u	0.09	$c_{\varepsilon 1}$	1.44
σ_t	0.9	$c_{\varepsilon 2}$	1.92
		$c_{\varepsilon 3}$	0.8

5 TEFLU Experiments

The experiment which is used here to investigate the performance of the two classes of turbulent heat flux models consists of a heated turbulent free jet of sodium in a highly turbulent multi-jet surrounding. The experiment was performed in the test facility TEFLU (Knebel 1993, Knebel et al. 1998). A similar experiment was performed earlier also in a water channel by Krebs (1979) and by Krebs et al. (1981). A schematics of the sodium test facility is shown in Fig. 2. The test section consisted of a pipe of $D=110$ mm diameter and a multi-bore jet block with 158 bores of $d=7.2$ mm diameter, placed on a triangular pitch of 8.2 mm. The length to diameter ratio for individual bores is 16.7.

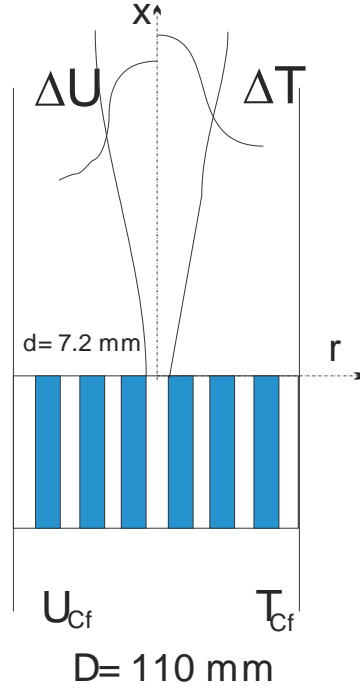


Figure 2: Sketch of a heated free jet in sodium behind a multi-bore jet block

Sodium was injected into the central bore with higher temperature ΔT and higher velocity ΔU than in the other bores. By modifying the ΔT , ΔU , and the co-flow velocity U_{cf} , three turbulent flow regimes were experimentally investigated with different buoyancy contributions: a forced jet, a buoyant jet, and a plume regime, see Table 4. These regimes were classified by the experimenters. The Reynolds number Re_{cf} is calculated using the co-flow velocities and the outer diameter D . Re_j is calculated using the maximum value of the velocity at the exit of the jet and the bore diameter d . The value of the densimetric Froude number at the exit of the jet block determines the flow regime:

$$Fr_j = \frac{(\overline{U}_j^2 - \overline{U}_{cf}^2) \rho_{cf}}{g(\rho_j - \rho_{cf})d}. \quad (23)$$

The subscripts j and cf refer to the exit of the jet and to the co-flow respectively and ρ indicates the density.

Radial profiles of mean velocity, mean temperature and variance of temperature fluctuations were measured at several positions downstream the jet block.

Table 4: Experimental conditions.

Experiment	\bar{u}_{cf} (m/s)	T_{cf} (K)	Re_{cf}	$\Delta \bar{u}_j$ (m/s)	ΔT_j (K)	Re_j	Fr_j
a) forced jet	0.05	573	1.4×10^4	0.50	30	1.01×10^4	521
b) buoyant jet	0.1	573	2.8×10^4	0.33	25	7.9×10^3	365
c) plume	0.1	573	2.8×10^4	0.17	75	4.96×10^3	43.1

6 FLUTAN Calculations

6.1 Numerical Model Specifications

6.1.1 Geometry and Boundary Conditions

With nowadays computer capabilities it is still not practicable to record all the bores in the block and the jets in the outer pipe together with sufficient spatial resolution. Therefore, a computational domain was chosen which only models part of the jet area in the pipe. So, the grid records the fluid domain downstream the jet block starting from the plane $x/d=6$ for an axial length of 400 mm. By using symmetry conditions only half of the tube is modeled, from the axis to the wall. After parametric investigations a two-dimensional numerical grid composed by 19,200 cells (64x1x300) in an cylindrical axis-symmetric geometry was found as reference grid which is sufficient to obtain a grid independent solution. This grid is used for all three regimes. The mesh size of the grid changes from 0.36 mm to 1.44 mm in the radial direction and from 0.72 mm to 2.88 mm in the axial direction.

The inlet profiles play an important role in such calculations, especially as the computational domain begins in an area with inhomogeneous flow data. A more detailed discussion of the problem with the inlet conditions for this type of flow is given in Carteciano (1996). The inlet profiles for mean velocity, mean temperature, and variance of temperature fluctuations were determined from measured values. The other turbulence quantities described by separate transport equations also need inlet specifications, but directly measured data are not available from TEFLU. The inlet profiles for k were deduced from analogous experiments performed by Corrsin (1943) with air using similarity considerations:

$$k_s(r) = k_a(r) \frac{\overline{u_s^2}(r)}{\overline{u_a^2}(r)} . \quad (24)$$

The subscripts s and a refer to sodium and air respectively and \overline{u} indicates the inlet normal velocity. This procedure becomes inappropriate with increasing buoyancy effects. However, because of the lack of better approximation possibilities it will be applied in all three regimes. The inlet profiles for ε are calculated from the k profiles using the following relation based on the equilibrium of production and dissipation of turbulence energy in a fully developed flow:

$$\varepsilon = c_\mu k^2 / v_t . \quad (25)$$

Here a mean value of v_t is deduced from the air experiments by using similarity considerations. The estimated ε profiles were modified on the basis of calculations performed by Bunk et al. (1995) in order to obtain a correct inlet momentum flux.

The uncertainty regarding the inlet boundary conditions of the turbulence quantities should be considered as an important topic to be analyzed, because the numerical results

are strongly depending on the inlet boundary conditions. The topic of our calculations is to compare and benchmark the turbulence models implemented in FLUTAN: therefore, we do not consider the uncertainty due to the inlet boundary conditions and we accept the inlet boundary condition given for the benchmark within the BWG (Maciocco 2000). This means, we do not try to improve the results by modifying the inlet conditions because we think it is not meaningful to circumvent the well-known jet-anomaly of the k- ϵ model by artificially adapting the inlet conditions. We instead adapt the value for c_μ to 0.06 as it is usually done for jet flows.

The complete data set used for the inlet profiles of the normal velocity, the mean temperature, the variance of temperature fluctuations, the turbulent kinetic energy, and its dissipation rate are shown in Tables 5-7 for all three regimes.

The inlet profiles for ϵ_T and for the turbulent heat fluxes were calculated using following empirical relationships (Carteciano 1996):

$$(\epsilon_T)_{\text{inl}} = \left(\overline{T'^2} \epsilon / k \right)_{\text{inl}} ; \quad (26)$$

$$\left(\overline{u'_x T'} \right)_{\text{inl}} = -0.1 (\partial T / \partial x)_{\text{inl}} . \quad (27)$$

Equation (26) is based on the local equilibrium of production and dissipation of turbulence energy in a fully developed flow, and equation (27) is following from eq. (21).

6.1.2 Physical and Numerical modeling

The turbulence models employed here are the TMBF and the standard k- ϵ - σ_t turbulence models. Both are used with their standard values for the model coefficients, except for some modifications which are specially mentioned in the results chapter. The TMBF is used in its full version, including the transport equation (17) for the dissipation rate of the temperature variance ϵ_T , instead of using the simpler model (16) which includes the unknown time scale ratio R , which would need adaptation to the special flow type and to the fluid. The dissipation or destruction rate of the heat fluxes $\epsilon_{U'T'}$ is modeled using the new modeling (19) instead of using (13), and the production term P_{eb} in the dissipation equation is modeled also according to the new model, equation (18), instead of using equation (8).

In the standard k- ϵ - σ_t model the turbulent Prandtl number has to be prescribed. Here we are not interested in optimizing or investigating the performance of this model for liquid metals, but in using it in a manner as most users do it: I.e., we use the standard value of $\sigma_t = 0.9$ in all calculations with this first order model in this report.

The calculations were performed with the first order upwind discretization method for the convective terms in the momentum, energy, and turbulence equations. A first order time discretization was used with $\Delta t = 0.1$ s. The system of transport equations is solved by a direct GAUSS-Solver. The numerical solution of higher order turbulence models with a larger number of transport equations may be problematic. Here, a very low value for the convergence criterion parameter was chosen for the outer iteration loop to calculate the material property data etc.: 10^{-7} . The steady state is reached when the change of each

velocity component divided by the maximum velocity magnitude and the change of the enthalpy divided by the maximum enthalpy value in the entire field are less than 10^{-7} .

6.2 Results

6.2.1 Forced Jet

Experience has shown that the radial spreading of an axi-symmetric jet in forced convection is over-predicted by about 20 to 30 per cent (in the case of a stagnant ambient flow) when the standard value of the empirical coefficient $c_{\mu}=0.09$ in the $k-\varepsilon$ model is used (Rodi 1980). The coefficient c_{μ} must be corrected by a function of suitable flow parameters. This function is not implemented in FLUTAN but the mean velocity field calculated by the $k-\varepsilon-\sigma_t$ model and by the TMBF model shows a satisfactory agreement with the experiment when the value of $c_{\mu}=0.06$ is used (Figs. 3 and 4). The TMBF and the $k-\varepsilon-\sigma_t$ model give the same numerical results in predicting the velocity field. In fact, both models describe the turbulent transport of momentum using the same transport equations for k and ε . The main difference in this description is the modeling of the buoyancy term (eq. 14 and eq. 22) which is, as expected, of negligible magnitude in this forced jet regime.

The radial temperature profiles predicted by the $k-\varepsilon-\sigma_t$ model are flatter than the measured one (Fig. 5) due to an over-estimation of the radial heat transport from the axis to the outer flow. In contrast, the mean temperature field is better predicted by the TMBF (Fig. 6) which calculates a smaller turbulent heat flux in the radial direction than the one calculated by the $k-\varepsilon-\sigma_t$ model (Fig. 7).

The TMBF also provides results for the variance of temperature fluctuations $\overline{T'^2}$. The calculated data meet the experimental data quite well, Fig. 8. This agreement is achieved by using the transport equation for ε_T following eq. (17) instead of using a modeled sink term ε_T according to eq. (16) in the equation for the variance of temperature fluctuations.

6.2.2 Buoyant Jet

In contrast to the forced jet, the calculated velocity field for the buoyant jet agrees satisfactorily with the experimental one when the standard value of $c_{\mu}=0.09$ is used (Figs. 9 and 10). No reduction of the value of c_{μ} is needed in this case. This is probably due to the smaller ΔU_j (0.33 m/s versus 0.5 m/s) and due to the higher value of the co-flow velocity (0.1 m/s versus 0.05 m/s). The fact that the TMBF simulates the same velocity field calculated by the $k-\varepsilon-\sigma_t$ model means that the influence of buoyancy on the velocity field is still negligible.

As in the forced regime, the radial spreading of the temperature profile is overestimated by the $k-\varepsilon-\sigma_t$ model (Fig. 11). The mean temperature field is well reproduced by the TMBF (Fig. 12) which calculates a lower radial heat transport by turbulence (Fig. 13). However, it must be noted that the overestimation of the radial heat transport by the $k-\varepsilon-\sigma_t$ model is now reduced in comparison with the forced jet.

An astonishingly good agreement between the calculated $\overline{T^2}$ and the experimental data is again achieved by using the TMBF (Fig. 14); these data usually react very sensitive against any deficiencies of the model or of the inlet conditions.

6.2.3 Plume

As a confirmation of the results for the buoyant jet, the experimental velocity field is again properly simulated using the standard value of $c_\mu=0.09$: ΔU_j is in the plume regime further reduced to 0.17 m/s. The TMBF and the $k-\varepsilon-\sigma_t$ model calculate again the same velocity field (Figs. 15 and 16). This result signalizes that the temperature influence on the velocity field due to the turbulent transport of heat is still negligible, whereas this regime was classified as plume by the experimenters.

In contrast to the calculations for the forced and buoyant jet, the radial temperature profiles are well simulated by both models, even if a better agreement to the experiment is reached by the TMBF for the profile at $x/d=11$, Figs. 17 and 18. However, the TMBF still calculates lower values of the radial turbulent heat flux like in the previous cases (Fig. 19). An explanation for this result will be given in the next chapter.

The radial profiles of $\overline{T^2}$, which can be calculated by the TMBF, are in this case clearly overestimated (Fig. 20). This calculation and the analysis of direct numerical simulation data for convection in several fluids by Wörner & Grötzbach (1996) and Wörner et al. (1999) shows that the standard set of empirical coefficients for the transport equation for ε_T is not sufficient for getting a good agreement with the experimental field of the temperature variances at small Prandtl numbers. Thus, either corrective functions depending on the Peclet number should be developed for some coefficients in this equation. Or, the new formulation for the transport equation for ε_T developed by using the two-point correlation technique by Otic (Grötzbach et al. 2002b, Otic & Grötzbach 2003) should be investigated instead.

7 Discussion

The TMBF and the $k-\varepsilon-\sigma_t$ model can adequately simulate the turbulent transport of momentum using the standard values of the empirical coefficients for the buoyant jet and for the plume regime. However, the value of c_μ must be reduced to 0.06 in the case of the forced jet in order to damp the well known attitude of the $k-\varepsilon$ model to overestimate the radial spreading of an axi-symmetric jet. The fact that the TMBF simulates the same velocity field as calculated by the $k-\varepsilon-\sigma_t$ model signalizes that the temperature influence on the velocity field by means of the turbulent transport of heat is negligible even in the case of the plume regime. In fact, both models describe the turbulent transport of momentum using essentially the same transport equations of k and ε . The main difference in this description is in the model of the buoyancy term which is obviously of negligible order in all the calculations.

The TMBF is a significant improvement in comparison to the $k-\varepsilon-\sigma_t$ model in the simulation of the turbulent transport of heat. The TMBF can reproduce the mean temperature field well by using the standard values of empirical coefficients in all experiments. This good agreement is due to the separate treatment of the turbulent

transport of heat and momentum in the TMBF using the transport equations for the three heat fluxes instead of using the isotropic Fourier assumption. In contrast, the $k-\varepsilon-\sigma_t$ model cannot accurately simulate the mean temperature field when the standard turbulent Prandtl number is used. As a result of a strong anisotropy in the field of the temperature gradient which shows very high values perpendicular to the flow direction, the turbulent heat flux acting perpendicular to the flow direction has very high values when the heat fluxes are calculated setting them proportional to the temperature gradient as in the first order models which use the Fourier assumption. For this reason the $k-\varepsilon-\sigma_t$ model gives an unsatisfactory prediction of the turbulent heat fluxes overestimating the values compared with the TMBF.

The fields of σ_t can be calculated by the TMBF (Fig. 21). They represent approximate values because σ_t is calculated using the turbulent heat fluxes, which are modeled by transport equations, and the turbulent shear stresses, which are modeled like in the $k-\varepsilon$ model by velocity gradients. The calculated turbulent Prandtl number has higher values than the standard one of $\sigma_t = 0.9$, which is used by the calculation with the $k-\varepsilon-\sigma_t$ model. Moreover, it is not constant. It depends not only on the fluid, what is well known (Kays 1994), but also on the flow regime and on the position. The $k-\varepsilon-\sigma_t$ model can give good results only by adjusting the value of σ_t reducing the turbulent heat flux acting perpendicularly to the flow direction (Carteciano 1995).

The influence of the overestimation of the turbulent radial heat flux on the temperature field by the $k-\varepsilon-\sigma_t$ model becomes negligible in the plume regime because the turbulent conductivity Γ_t , which is in all three flow regimes lower than the molecular one, which is $\Gamma = 76 \text{ W}/(\text{m K})$, is reduced from the forced jet to the plume regime (see Fig. 22). Therefore, the heat transport by turbulence becomes less and less important compared with the molecular one going from the forced flow to the plume regime. This explains the good prediction of the temperature field performed by the $k-\varepsilon-\sigma_t$ model in case of the plume regime.

The TMBF adequately simulates the variance of temperature fluctuations $\overline{T'^2}$ in two experiments but not in the plume regime. Due to the use of a transport equation for ε_T , the spatial distribution of the problematic value of the turbulent time-scale ratio

$$R=0.5*(\overline{T'^2}/\varepsilon_T)/(k/\varepsilon) \quad (28)$$

can be analyzed from the calculations using equations (16) or (28) which is otherwise needed on input to model the sink term in the $\overline{T'^2}$ equation; this is also important for the new model term in the transport equations for the heat fluxes, see eq. (18). The different values calculated for R in each experiment show that R depends not only on the molecular Prandtl number and on the position, but also on the Reynolds number (Fig. 23). The results for the plume are surprisingly large; they suffer from the problem that the temperature variances are badly reproduced by the TMBF in this case.

There exist no data for R which are determined by direct measurements of the quantities appearing in eq. (28), because the dissipative range of the spectrum can only be resolved by modern sensors for a few flows and only at small Reynolds numbers; instead most data from experiments are determined by some modeling assumptions. So, for this peculiar type of flow and fluid Bremhorst et al. (1989) and Gehrke & Bremhorst (1993) deduced R data in the order of about 0.4, what is larger than analyzed from the TMBF results. Instead, most directly determined R data are coming from the analysis of DNS results. For forced convection in a heated plane channel Kawamura et al. (1998, 1999)

gives data for a somewhat larger Prandtl number, $Pr = 0.025$, of below or around 0.2. He finds that this value depends only weakly on Re , but more strongly on Pr and wall distance. For Rayleigh-Bénard convection for several liquid metals Grötzbach & Wörner (1992), Wörner (1994), Wörner & Grötzbach (1995), and Grötzbach & Otic (2002) give R data from their DNS; the data depend at small Prandtl numbers on Prandtl number, Rayleigh number, and wall distance. The values found here by the TMBF are with $R < 0.2$ roughly in that range as it was found in the DNS for liquid sodium. So, the problem of getting reliable data for R gets obvious from this comparison. Currently a model is under development to describe the profiles of R at least for Rayleigh-Bénard convection in fluids with a wide range of Prandtl numbers (Otic 2003). Such a model should allow for more accurate calculations and to avoid the solution of the additional transport equation for ε_T with its many models and coefficients.

8 Conclusions

FLUTAN calculations of a turbulent hot jet of sodium are performed for three different buoyancy regimes called forced jet, buoyant jet, and plume. The jet flow has the advantage that the calculated turbulent mixing only depends on the turbulence models used, and perhaps also on the numerical schemes, but not on any wall models like wall functions. Two different turbulence models are used: the standard $k-\varepsilon-\sigma_t$ model and a combination of a standard $k-\varepsilon$ model with a full second order heat flux model called Turbulence Model for Buoyant Flows (TMBF).

The calculations of the TEFLU experiments show the limits of the applicability of an eddy diffusivity approach used by the $k-\varepsilon-\sigma_t$ model to liquid metal flows. Whereas the calculated velocity fields are in close agreement with the measurements, the calculated temperature profiles are only in those cases acceptable in which the heat fluxes are more or less governed by the molecular diffusivity. The TMBF which is a compromise between the classical $k-\varepsilon-\sigma_t$ model and the Reynolds stress model is clearly an improvement of the $k-\varepsilon-\sigma_t$ model for turbulent flows in which the turbulent transport of heat is complex and the Reynolds analogy is not valid, such as in liquid metal flows. In all cases, the temperature fields calculated by the TMBF agree better with the measured data. The TMBF does already contain some specific model extensions which were deduced from direct numerical simulations for turbulent liquid metal convection. Further improvements of the TMBF are still necessary for liquid metal flows to reduce the overestimation of the radial profiles of $\overline{T'^2}$ in the plume regime. The inclusion of the Peclet number dependency in the transport equation of ε_T (Wörner et al. 1996 and 1999) should lead to physically sound results. An alternative could be to use the new formulation with an improved modeling for the dissipation of thermal variances ε_T as currently deduced by Otic (Otic & Grötzbach 2003).

Even though the FLUTAN predictions agree well with experimental data, further validation of the TMBF is needed especially for liquid metal flow regimes in which the calculated fields are mainly determined by the turbulent heat transport and not by the molecular one.

One should keep in mind that the range of validity of the TMBF could be restricted by the assumption of isotropy of the eddy viscosity ν_t whereas anisotropy is included in the calculated turbulent heat fluxes. Such anisotropy in the eddy viscosity may become

important in 3-D flows and near walls. For these kinds of flows, at least Algebraic Stress Model (ASM) extensions for the two-equation Reynolds stress models should be used, Table 1. Such a model would combine the necessary features to include anisotropic eddy diffusivities and an accurate heat flux modeling together with an acceptable numerical effort and with robustness.

References

- Ammann, T., 1997. Entwicklung eines impliziten Verfahrens zur lokalen Verfeinerung eines strukturierten Gitters. Dissertation, Universität Karlsruhe, FZKA 5864, Forschungszentrum Karlsruhe.
- Baumann, W., Carteciano, L., Weinberg, D., 1997. Thermal propagation effects in a vertical turbulent flow behind a jet block - A benchmark exercise. J. of Hydraulics Research, Vol. 35, pp. 843-864.
- Borgwaldt, H., 1990. CRESOR, A robust vectorized Poisson solver implemented in the COMMIX-2(V) thermal-hydraulic code. Int. Conf. On Supercomputing in Nuclear Applications (SNA 90). Mito City, Japan, March 12-16, 1990, pp. 346-351.
- Bottoni, M., Baumann, W.L., Chi, H.N., Chien, T.H., Domanus, H.M., Schmitt, R.C., Sha, W.T., Shah, V.L., 1985. COMMIX-2: A three-dimensional transient computer program for thermal-hydraulic analysis of two-phase flows. NUREG/CR-4371, ANL-85-47.
- Bottoni, M., Willerding, G., 1987. Advanced solution algorithms for transient multidimensional thermohydraulic flow problems in complex geometries with the program COMMIX-2/KfK. Nuclear Engineering and Design, Vol. 100, pp.351-365.
- Bremhorst, K., Krebs, L., Müller, U., Listijono, J.B.H., 1989. Application of a gradient diffusion and dissipation time scale ratio model for prediction of mean and fluctuating temperature fields in liquid sodium downstream of a multi-bore jet block. Int. J. Heat Mass Transfer, Vol. 32, pp. 2037-2046.
- Bunk, M., Hoelle, C., Knebel, J.U., Müller, U., 1995. Berechnung von Auftriebsströmungen mit dem $k-\varepsilon-\overline{T^2}$ -Turbulenzmodell. FZKA 5519, Forschungszentrum Karlsruhe.
- Carteciano, L.N., 1995. Analysis of a turbulence model for buoyant flows implemented in the 3d thermal-hydraulic computer code FLUTAN and comparison with the standard $k-\varepsilon-\sigma_t$ model. Turbulence, Heat and Mass Transfer 1. Ed. K. Hanjalic, J.C.F. Pereira, Begell House, Inc. Publishers; New York, pp. 222-227.
- Carteciano, L.N., 1996. Entwicklung eines Turbulenzmodells für Auftriebsströmungen. Dissertation, Universität Karlsruhe, FZKA 5775, Forschungszentrum Karlsruhe.
- Carteciano, L.N., Weinberg, D., Müller, U., 1997. Development and analysis of a turbulence model for buoyant flows. 4th World Conference on Experimental Heat Transfer, Fluid Mechanics and Thermodynamics. Bruxelles, June 2-6, Vol.3, pp. 1339-1347.
- Carteciano, L.N., Wörner, M., Grötzbach, G., 1999. Erweiterte Turbulenzmodelle für technische Anwendung von FLUTAN auf Naturkonvektion. Jahrestagung Kerntechnik 99, Karlsruhe, May 18-20, pp.129-134.

- Carteciano, L., Dorr, B., Grötzbach, G., Olbrich, W., Jin, X., 2001. Two- and three-dimensional thermal and fluid-dynamical analysis of the complete MEGAPIE-module with the computer code FLUTAN. Programm Nukleare Sicherheitsforschung, Jahresbericht 2000, Forschungszentrum Karlsruhe, FZKA 6653, pp. 443 – 458.
- Cheng, X., Müller, U., 1998. Turbulent natural convection coupled with thermal radiation in large vertical channels with asymmetric heating. *Int. J. Heat Mass Transfer* 41, pp. 1681-1692.
- Corrsin, S., 1943. Investigation of flow in an axially symmetric heated jet of air. NACA wartime report, W-94.
- Gehrke, P.J., Bremhorst, K., 1993. Lateral velocity fluctuations and dissipation time scale ratios for prediction of mean and fluctuating temperature fields. *Int. J. Heat Mass Transfer*, Vol. 36, pp. 1943-1952.
- Gibson, M.M. and Launder, B.E., 1978. Ground effect on pressure fluctuations in the atmospheric boundary layer. *J. Fluid Mech.*, Vol. 86, pp. 491-511.
- Grötzbach, G., Otic, I., 2002. Simulation of turbulent convection in low Prandtl-number fluids. 9th International Conference on Numerical Methods and Computational Mechanics 2002 (NMCM 2002), University of Miskolc, Hungary, 15.-19.7.2002, HU ISBN 963 661 535 7, pp. 91-92.
- Grötzbach, G., Wörner, M., 1992. Analysis of second order transport equations by numerical simulations of turbulent convection in liquid metals. Proc. 5th International Topical Meeting on Nuclear Reactor Thermal Hydraulics (NURETH-5), American Nuclear Society, LaGrange Park, Ill., Vol. II. pp. 358-365.
- Grötzbach, G., Carteciano, L.N., Dorr, B., 2002a. Numerical analysis of experiments modelling LWR sump cooling by natural convection. In.: *Natural Circulation Data and Methods for Advanced Water Cooled Nuclear Power Plant Design*, IAEA-TEC-DOC-1281, pp. 195 – 206.
- Grötzbach, G., Batta, A., Drummond, R., Otic, I., Panefresco, C., 2002b. Fundamental Experiments in Liquid Lead-Bismuth on Heat Transfer and Model Development / Model Validation. Programm Nukleare Sicherheitsforschung, Jahresbericht 2001, Forschungszentrum Karlsruhe, FZKA 6741, pp. 429 – 436.
- Günther, C., 1992. Fortgeschrittene Upwind-Differenzenverfahren zur numerischen Lösung der Konvektions-Diffusionsgleichung. Habilitation, Universität Karlsruhe, KfK 4697, Kernforschungszentrum Karlsruhe.
- Hanjalic K., 1994. Achievements and limitations in modelling and computation of buoyant turbulent flows and heat transfer. 10th Int. Heat Transfer Conference, Brighton, Vol. 1, pp. 1-18.

- Jin, X., 2001. Rechenverfahren zur Diskretisierung von Strömungen in komplexer Geometrie mittels körperangepasster Gitter. Dissertation, Universität Karlsruhe, FZKA 6596, Forschungszentrum Karlsruhe.
- Jones, W.P., Launder, B.E. , 1972. The prediction of laminarization with a two-equation model of turbulence. *Int. J. Heat Mass Transfer*, Vol. 15, pp. 301-314.
- Kawamura, H., Ohsaka, K., Abe, H., Yamamoto, K., 1998, DNS of turbulent heat transfer in channel flow with low to medium-high Prandtl number fluid, *Int. J. Heat Fluid Flow* 19, 482-491
- Kawamura, H., Abe, H., Matsuo, Y., 1999, DNS of turbulent heat transfer in channel flow with respect to Reynolds and Prandtl number effects, *Int. J. Heat Fluid Flow* 20, 196-207
- Kays, W. M., 1994. Turbulent Prandtl number – Where are we ? (The 1992 Max Jakob Memorial Award Lecture). *J. of Heat Transfer*, Vol. 116, pp. 284 – 295.
- Knebel, J.U., 1993. Experimentelle Untersuchungen in turbulenten Auftriebsstrahlen in Natrium. Dissertation, Universität Karlsruhe, KfK 5175, Kernforschungszentrum Karlsruhe.
- Knebel, J.U., Krebs, L., Müller, U., Axcell, B.P., 1998. Experimental investigations of a confined heated sodium jet in a co-flow. *J. Fluid Mech.*, Vol. 368, pp. 51-79.
- Knebel, J.U., Cheng, X., Müller, G., Schumacher, G., Konys, J., Wedemayer, O., Grötzbach, G., Carteciano, L.N., 2000. Thermalhydraulic and material specific investigations into the realization of an accelerator driven system (ADS) to transmute minor actinides. FZKA 6506, Forschungszentrum Karlsruhe.
- Krebs, L., 1979. Ausbreitung von Temperaturstörungen in begrenzter Strömung hinter einem Düsenblock.. Dissertation, Universität Karlsruhe, KfK 2846, Kernforschungszentrum Karlsruhe.
- Krebs, L., Bremhorst, K., Müller, U., 1981. Measurement and prediction of the mean and fluctuating temperature field downstream of a multi-bore jet block in which one jet is heated. *Int. J. Heat Mass Transfer*, Vol. 24, pp.1305-12.
- Launder, B.E., 1975. On the effect of a gravitational field on the turbulent transport of heat and momentum. *J. Fluid Mech.*, Vol. 67, pp. 569-581.
- Launder, B.E., 1978. Heat and mass transport in turbulence. *Topics in Appl. Phys.*, Ed.P.Bradshaw, Springer Verlag, Vol. 12.
- Leonard, B.P., 1979. A stable and accurate convective modelling procedure based on quadratic upstream interpolation. *Computer Methods in Applied Mechanics and Engineering*, Vol. 19, p. 59.

- Maciocco, L., 2000. Proposal for the benchmarking activity on the TEFLU sodium jet experiment. Personal information.
- Monin, A.S., 1965. On symmetry properties of turbulence in the surface layer of air. *Izv. Akad. Nauk. SSSR, Fizika atmosf. i.okeana*, Vol. 11.
- Moser, B., 1996. Entkopplung der Zeitintegration bei der Lösung der verschiedenen Erhaltungsgleichungen des Thermo-Fluiddynamikrechenprogramms FLUTAN. Diplomarbeit, Fachhochschule Stuttgart.
- Nagano, Y. and Kim, C., 1988. A two-equation model for heat transport in wall turbulent shear flows. *J. Heat Transfer*, Vol. 110, pp. 583-589.
- Nagano, Y., Shimada, M., Youssef, M. S., 1994. Progress in the development of a two-equation heat transfer model based on DNS databases. *Proc. Int. symposium on turbulence, heat and mass transfer*, Lissabon, Aug. 9-12, 1994, pp. 3.2.1-3.2.6.
- Olbrich, W., 2001. Personal information.
- Otic, I., 2003. Personal information.
- Otic, I., Grötzbach, G., 2003. Direct numerical simulation and statistical analysis of turbulent convection in lead-bismuth. *International Conference on Supercomputing in Nuclear Applications (SNA 2003)* Paris, Sept. 22-24, 2003.
- Prudhomme, C., 1998. Validierung eines Turbulenzmodells für Auftriebströmungen in Naturkonvektion, Diplomarbeit, Inst. für Kerntechnik und Reaktorsicherheit, Univ. Karlsruhe.
- Rodi, W., 1972. The prediction of free turbulent boundary layers by use of a two-equation model of turbulence. Ph.D. Thesis, Imperial College London.
- Rodi, W., 1980. Turbulence models and their application in hydraulics. MH DELFT, The Netherlands.
- Shikazono N. and Kasagi N., 1990. Modeling Prandtl number influence on scalar transport in isotropic and sheared turbulence. *Proc. 9th Symp. on Turbulent Shear Flows*, Kyoto, Japan, Vol. 2, pp. 18.3.1-18.3.6.
- Spalding, D.B., 1971. Concentration fluctuations in a round turbulent free jet. *Chem. Eng. Sci.*, Vol. 26, pp. 95-107.
- Willerding, G., Baumann, W., 1996. FLUTAN 2.0 Input specification. FZKA 5712, Forschungszentrum Karlsruhe.
- Wörner, M., 1994. Direkte Simulation turbulenter Rayleigh-Bénard-Konvektion in flüssigem Natrium, Dr. thesis, University Karlsruhe, KfK 5228, Forschungszentrum Karlsruhe.

- Wörner, M., Grötzbach, G., 1995. Analysis of thermal variance equation for natural convection of air and sodium. *Turbulence, Heat and Mass Transfer 1*, Ed. K. Hanjalic, J.C.F. Pereira, Begell House Inc., N.Y., pp. 332 – 337.
- Wörner, M., Grötzbach, G., 1996. Analysis of the transport equation of temperature variance dissipation rate by direct numerical simulation data of natural convection. *Engineering Turbulence Modelling and Experiments 3*, Eds.: W. Rodi, G. Bergeles, Elsevier Science B. V., pp. 229-238.
- Wörner, M., Grötzbach, G., 1997. DNS database of turbulent natural convection in horizontal fluid layers. World Wide Web-address <http://www.fzk.de/irs/turbit>.
- Wörner, M., Ye, Q.-Y., Grötzbach, G., 1999. Consistent modelling of fluctuating temperature-gradient-velocity-gradient correlations for natural convection. *Engineering Turbulence Modelling and Experiments 4*, Eds.: W. Rodi, D. Laurence, Elsevier Science B. V., pp. 165-174.
- Ye, Q.-Y., Wörner, M., Grötzbach, G., Jovanovic, J., 1997. Modelling turbulent dissipation rate for Rayleigh-Bénard convection. *Turbulence, Heat and Mass Transfer 2*, Eds.: K. Hanjalic, T.W.J. Peeters, Delft University Press, pp. 331-340.

Figures

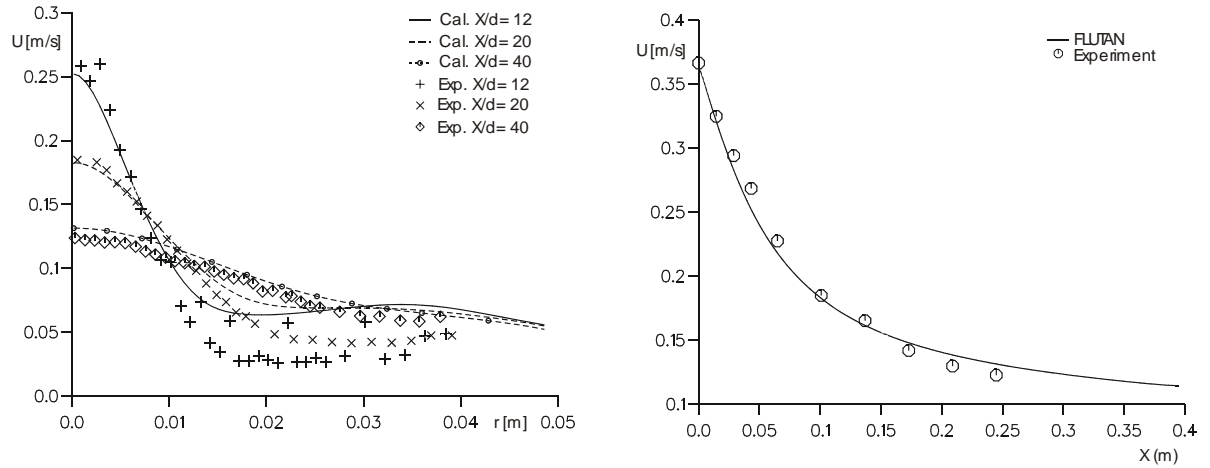


Figure 3: Forced Jet, radial velocity profiles at three different axial positions (left) and axial velocity profile at $r=0$ (right). Comparison between measurements and calculation with the $k-\varepsilon-\sigma_1$ model.

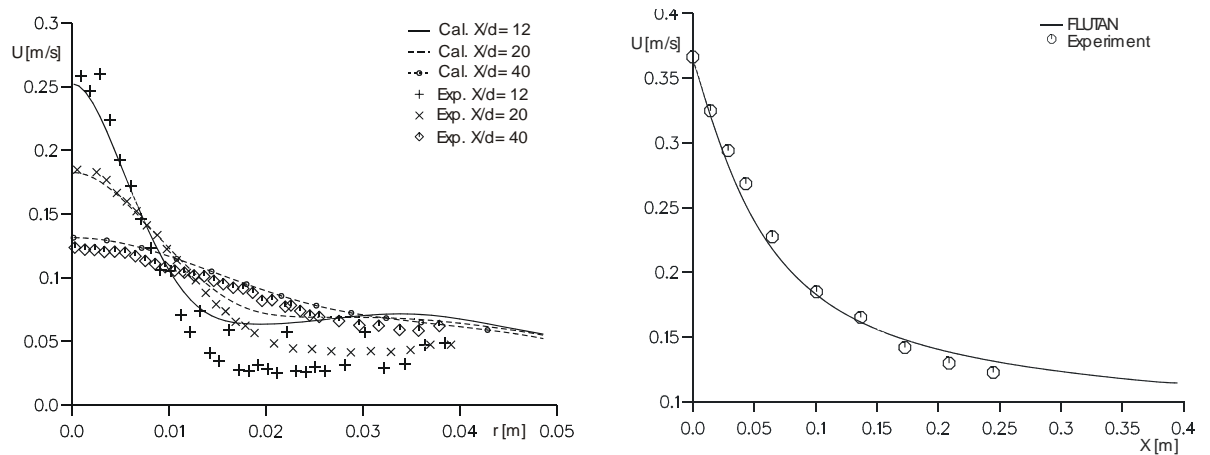


Figure 4: Forced Jet, radial velocity profiles at three different axial positions (left) and axial velocity profile at $r=0$ (right). Comparison between measurements and calculation with the TMBF model.

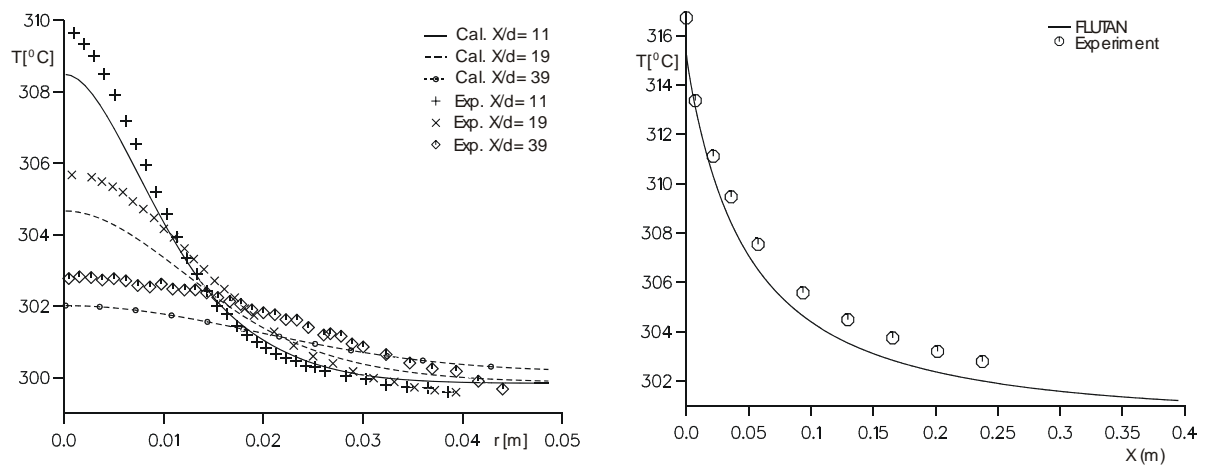


Figure 5: Forced Jet, radial temperature profiles at three different axial positions (left) and axial temperature profile at $r=0$ (right). Comparison between measurements and calculation with the $k-\epsilon-\sigma_T$ model.

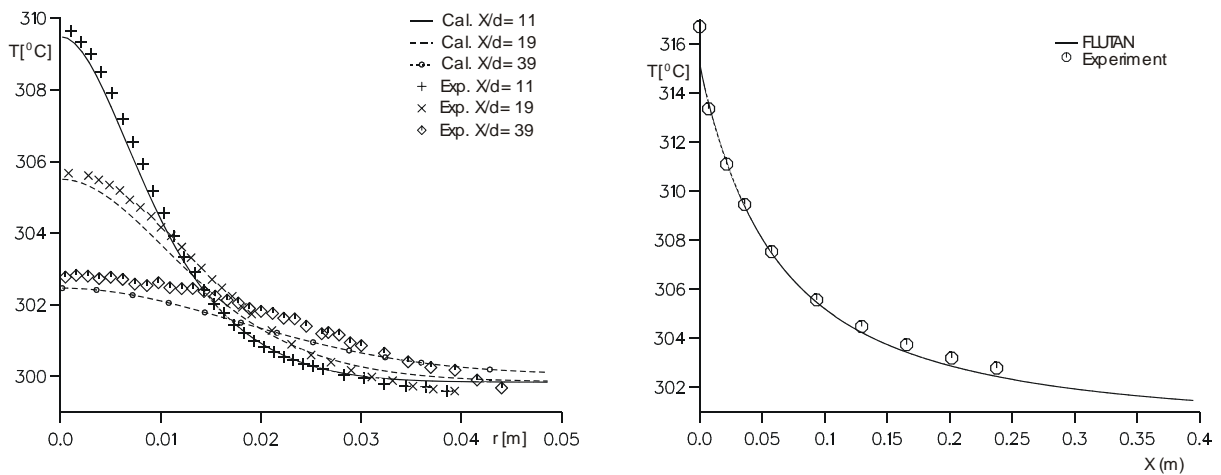


Figure 6: Forced Jet, radial temperature profiles at three different axial positions (left) and axial temperature profile at $r=0$ (right). Comparison between measurements and calculation with the TMBF model.

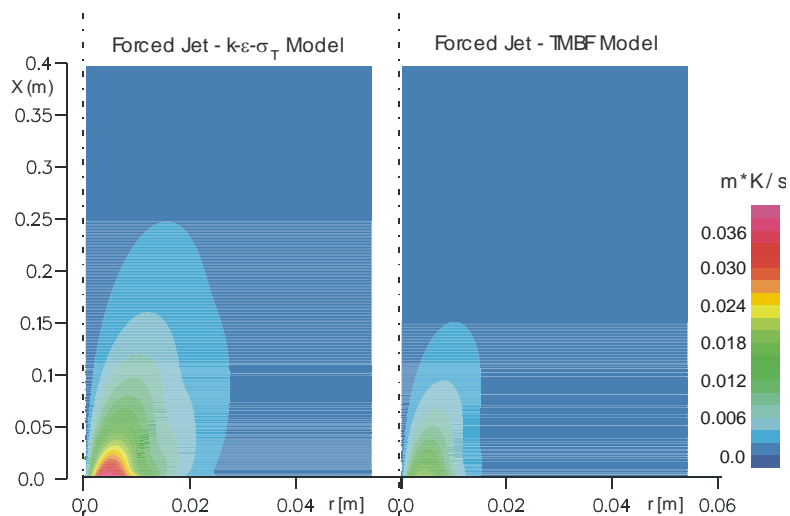


Figure 7: Forced Jet, calculated fields of the radial turbulent heat flux with the $k-\epsilon-\sigma_T$ model (left) and with the TMBF model (right).

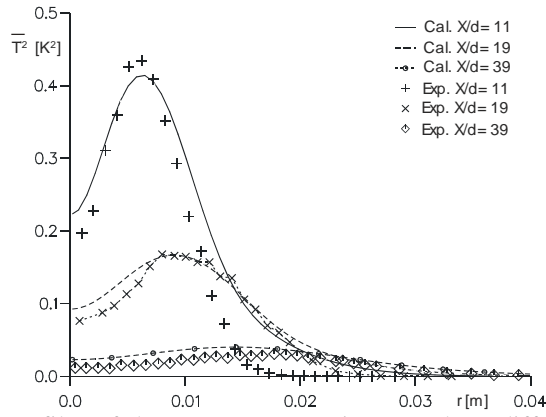


Figure 8: Forced Jet, radial profiles of the temperature variance at three different axial positions. Comparison between measurements and calculation with the TMBF model.

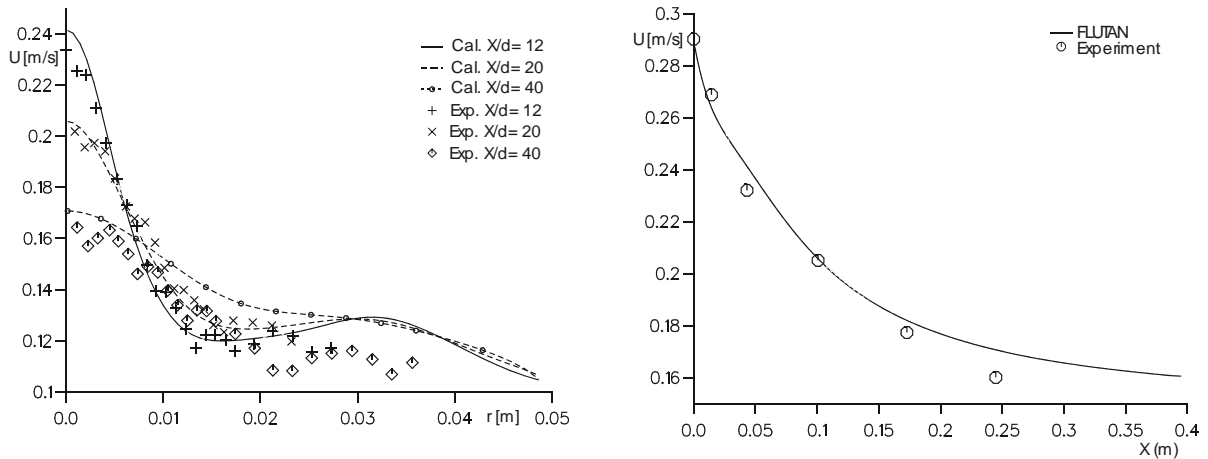


Figure 9: Buoyant Jet, radial velocity profiles at three different axial positions (left) and axial velocity profile at $r=0$ (right). Comparison between measurements and calculation with the $k-\epsilon-\sigma_t$ model.

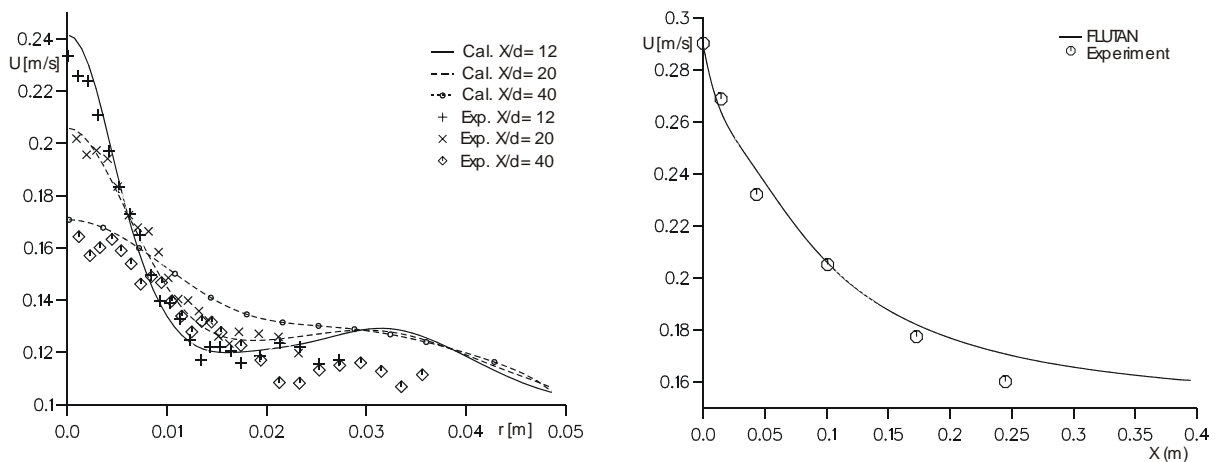


Figure 10: Buoyant Jet, radial velocity profiles at three different axial positions (left) and axial velocity profile at $r=0$ (right). Comparison between measurements and calculation with the TMBF model.

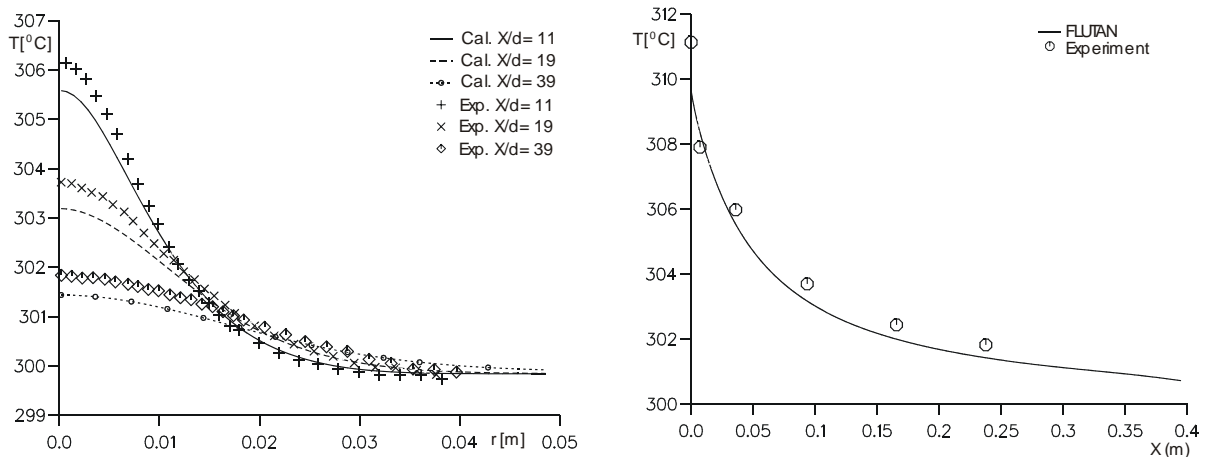


Figure 11: Buoyant Jet, radial temperature profiles at three different axial positions (left) and axial temperature profile at $r=0$ (right). Comparison between measurements and calculation with the $k-\epsilon-\sigma_t$ model.

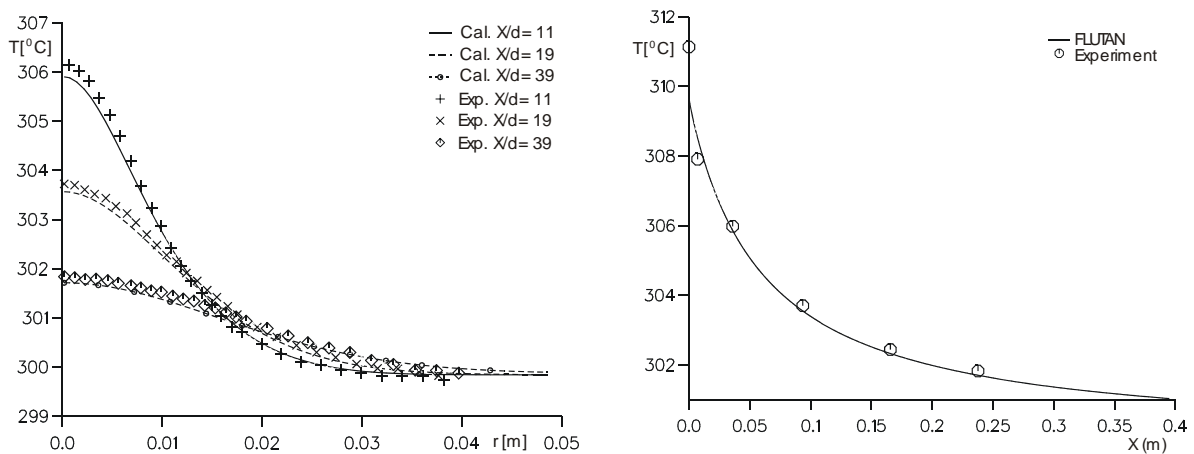


Figure 12: Buoyant Jet, radial temperature profiles at three different axial positions (left) and axial temperature profile at $r=0$ (right). Comparison between measurements and calculation with the TMBF model.

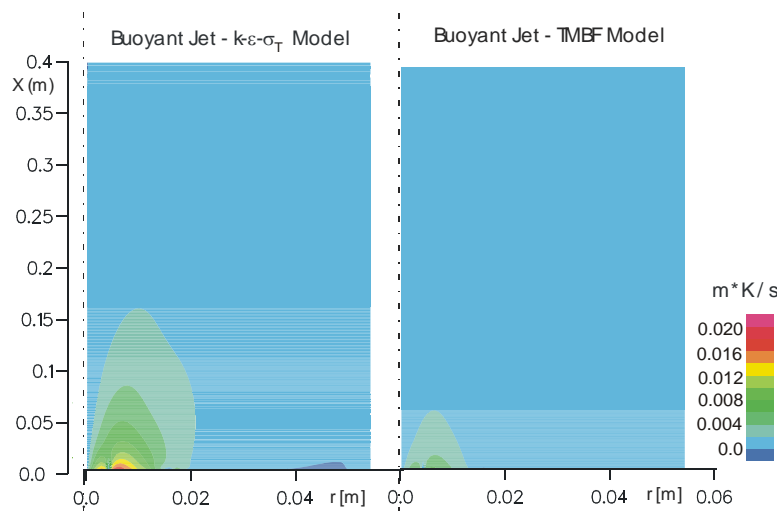


Figure 13: Buoyant Jet, calculated fields of the radial turbulent heat flux with the $k-\epsilon-\sigma_t$ model (left) and with the TMBF model (right).

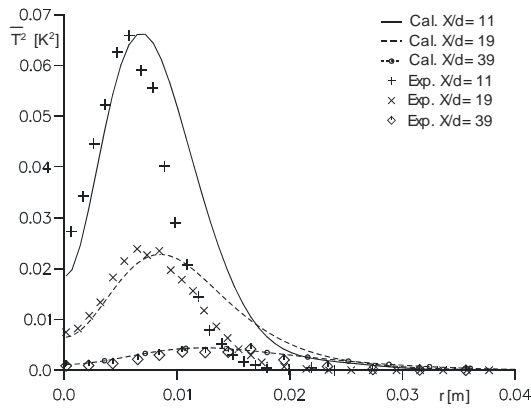


Figure 14: Buoyant Jet, radial profiles of the temperature variance at three different axial positions. Comparison between measurements and calculation with the TMBF model.

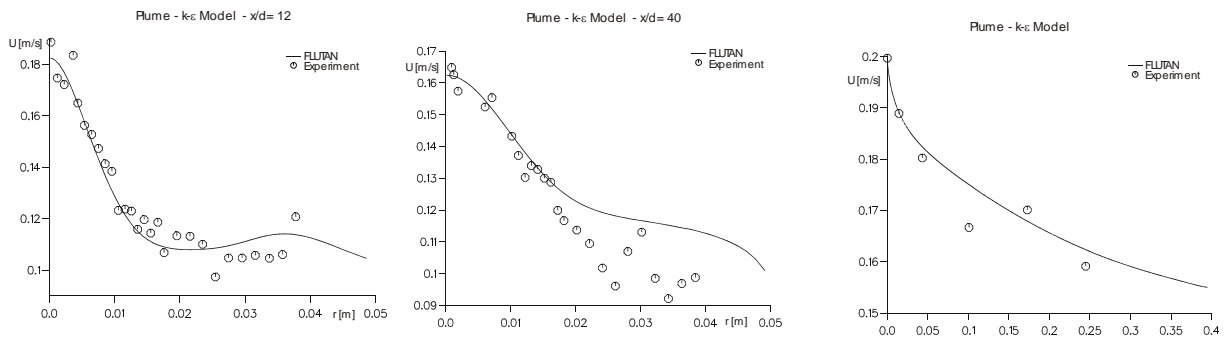


Figure 15: Plume, radial velocity profiles at two different axial positions (left and middle) and axial velocity profile at $r=0$ (right). Comparison between measurements and calculation with the $k-\epsilon-\sigma_t$ model.

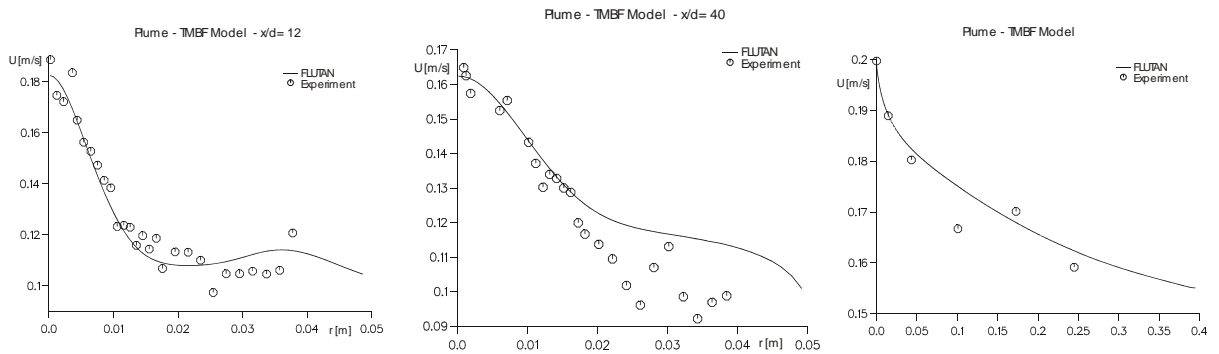


Figure 16: Plume, radial velocity profiles at two different axial positions (left and middle) and axial velocity profile at $r=0$ (right). Comparison between measurements and calculation with the TMBF model.

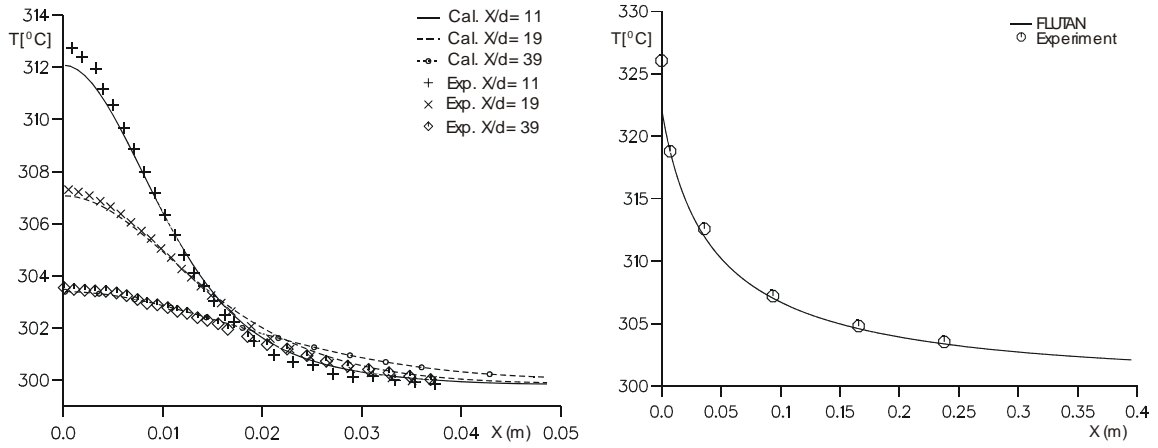


Figure 17: Plume, radial temperature profiles at three different axial positions (left) and axial temperature profile at $r=0$ (right). Comparison between measurements and calculation with the $k-\epsilon-\sigma_t$ model.

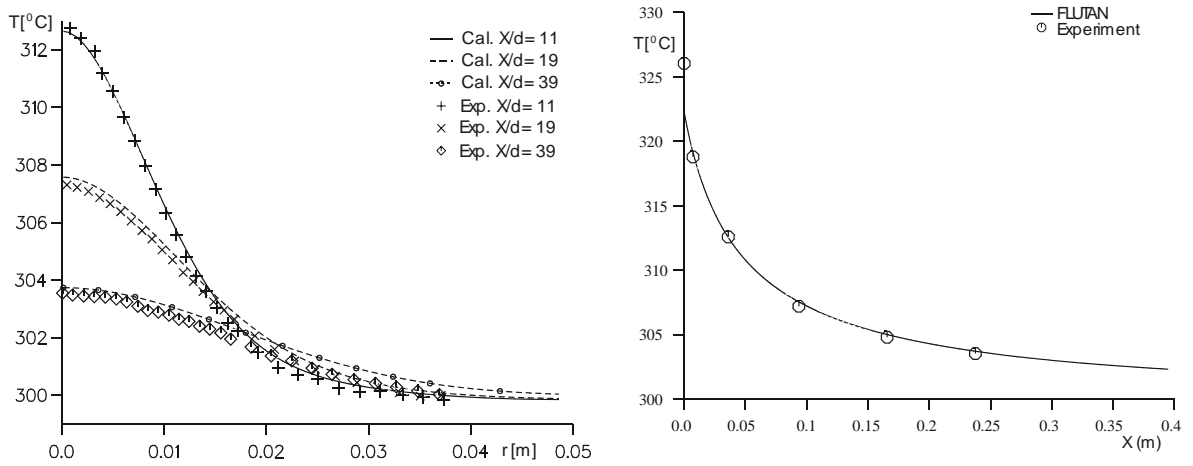


Figure 18: Plume, radial temperature profiles at three different axial positions (left) and axial temperature profile at $r=0$ (right). Comparison between measurements and calculation with the TMBF model.

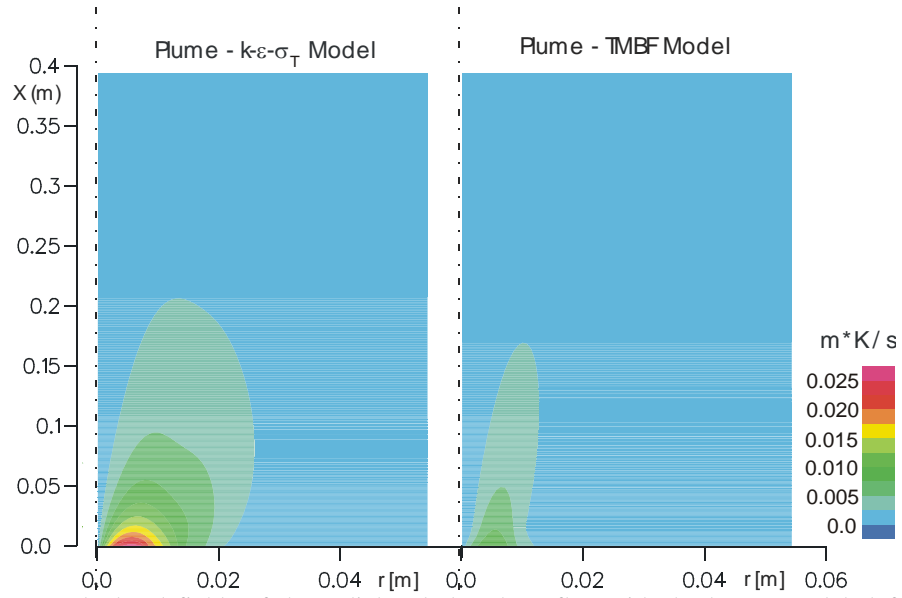


Figure 19: Plume, calculated fields of the radial turbulent heat flux with the $k-\epsilon-\sigma_t$ model (left) and with the TMBF model (right).

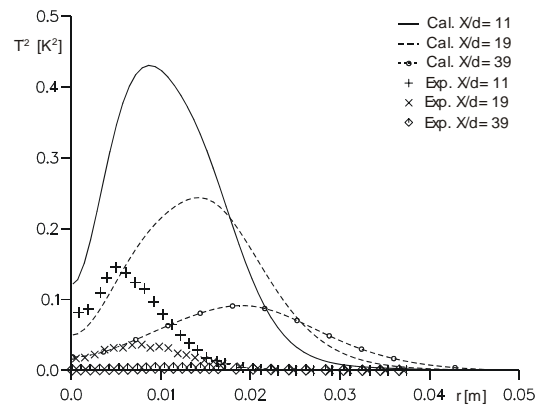


Figure 20: Plume, radial profiles of the temperature variance at three different axial positions. Comparison between measurements and calculation with the TMBF model.

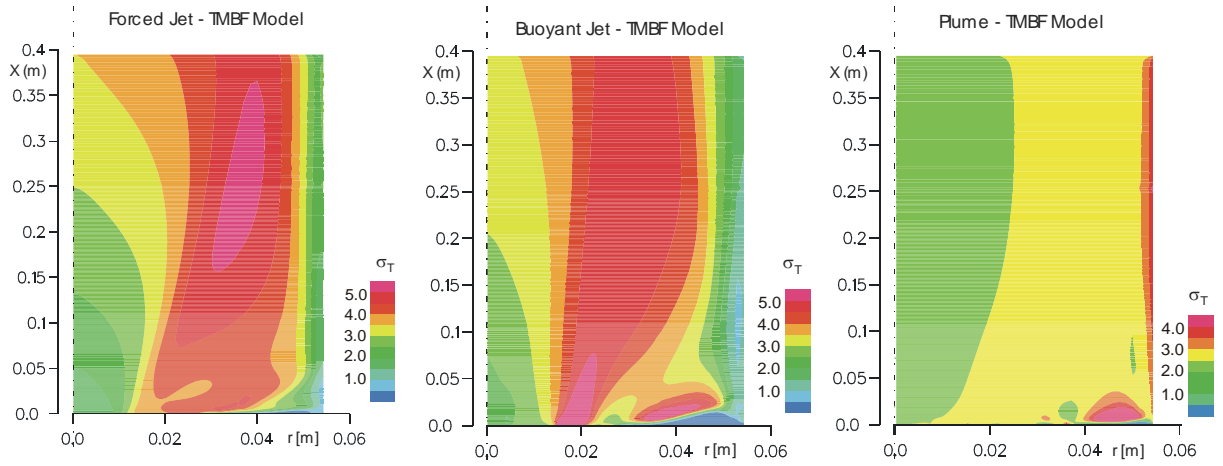


Figure 21: Field of the turbulent Prandtl number σ_t calculated with the TMBF model for the forced jet (left), buoyant jet (middle), and plume (right).

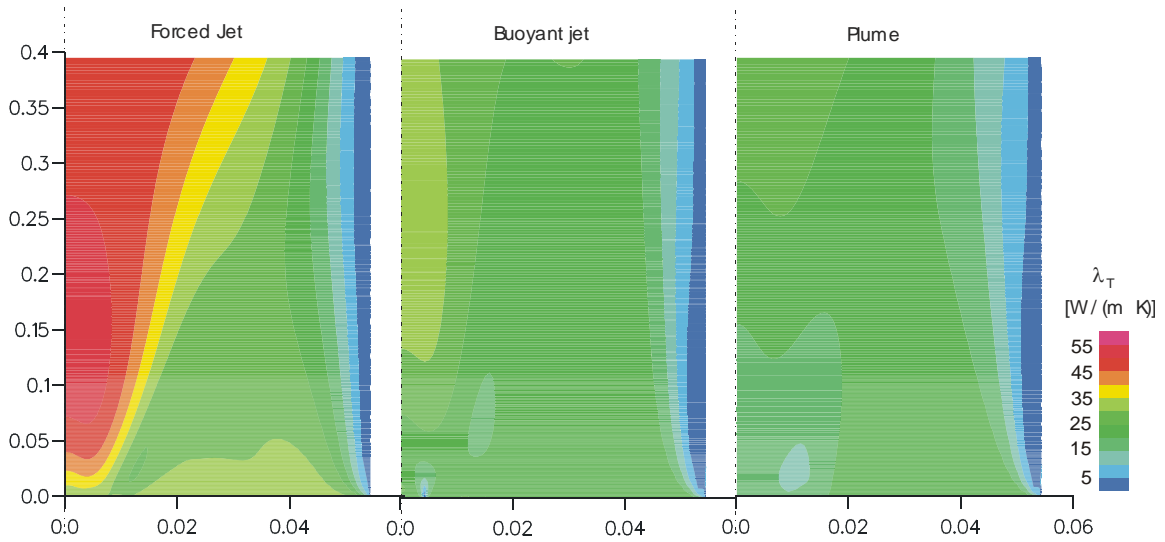


Figure 22: Field of the turbulent conductivity Γ_t calculated with the TMBF model for the forced jet (left), buoyant jet (middle), and plume (right).

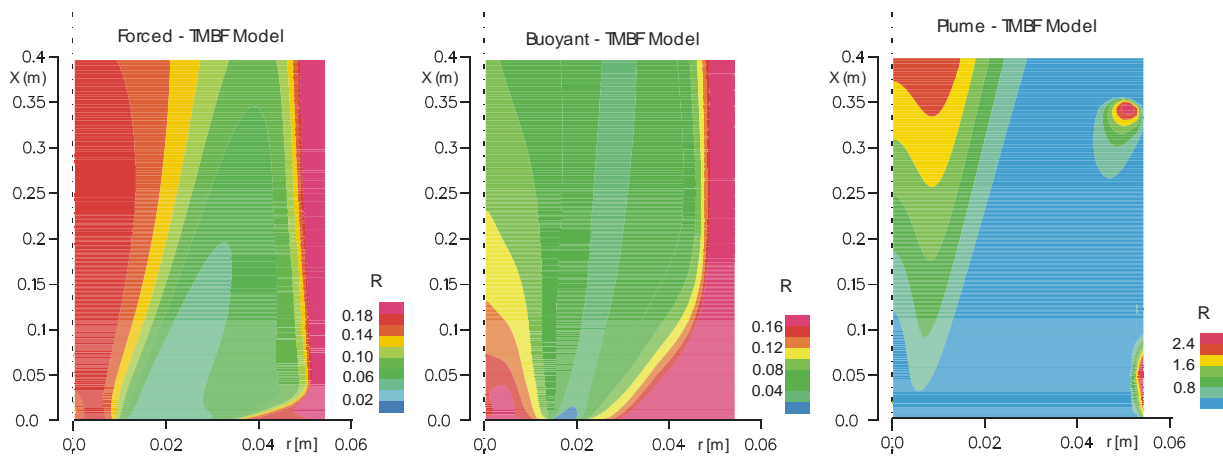


Figure 23: Field of the turbulent time-scale ratio R calculated with the TMBF model for the forced jet (left), buoyant jet (middle), and plume (right).

Tables

r/d	v (m/s)	T (K)	$\overline{T^2}$ (K ²)	k 10^4 (m ² /s ²)	ε 10^3 (m ² /s ³)
0	0.365	588.66	0.236	23	13
0.1	0.358	588.30	0.325	25.4	15.4
0.2	0.338	587.70	0.430	28.2	20.2
0.3	0.312	586.92	0.529	33	27
0.4	0.282	586.03	0.599	37.2	33.2
0.5	0.251	585.06	0.627	39.8	38.8
0.6	0.220	584.05	0.608	40	40
0.7	0.192	583.03	0.550	38	37
0.8	0.166	582.03	0.465	36	31
0.9	0.143	581.07	0.367	31	24
1	0.124	580.16	0.272	27	18
1.1	0.108	579.32	0.189	22	13
1.2	0.094	578.54	0.122	18	7.5
1.3	0.084	577.84	0.074	14	4.4
1.4	0.076	577.21	0.043	9.9	2.2
1.5	0.071	576.66	0.023	7	1.1
1.6	0.067	576.17	0.012	4.8	0.6
1.8	0.062	575.38	0.004	4.0	0.4
2	0.061	574.80	0.002	4.0	0.4
2.2	0.061	574.38	0.0005	4.0	0.4
2.4	0.061	574.06	0.000007	4.0	0.4
2.6	0.061	573.82	0.000001	4.0	0.4
2.8	0.062	573.63	0.000001	4.0	0.4
3	0.062	573.48	0.000001	4.0	0.4
3.4	0.064	573.16	0.000001	4.0	0.4
3.8	0.067	573	0.000001	4.0	0.4
4.2	0.071	573	0.000001	4.0	0.4
4.6	0.074	573	0.000001	4.0	0.4
5	0.077	573	0.000001	4.0	0.4
>7	0.050	573	0.000001	4.0	0.4

r/d	v (m/s)	T (K)	$\overline{T'^2}$ (K ²)	k 10 ⁴ (m ² /s ²)	ϵ 10 ³ (m ² /s ³)
0	0.294	582.95	0.0934	14	9.2
0.1	0.283	582.77	0.1054	14.5	10
0.2	0.269	582.45	0.1297	16	12
0.3	0.253	582.03	0.1548	18	16
0.4	0.237	581.51	0.1721	20	19
0.5	0.221	580.94	0.1767	22	23
0.6	0.205	580.32	0.1682	24	26
0.7	0.190	579.68	0.1495	24	27
0.8	0.176	579.04	0.1249	24	27
0.9	0.163	578.4	0.0989	23	24
1	0.152	577.79	0.0747	21	22
1.1	0.143	577.2	0.0543	19	18
1.2	0.135	576.66	0.0383	17	14
1.3	0.128	576.16	0.0264	15	11
1.4	0.124	575.7	0.0181	12	7.8
1.5	0.120	575.3	0.0123	11	5
1.6	0.117	574.95	0.0084	8.7	3.3
1.8	0.115	574.4	0.0041	6.8	2.2
2	0.116	574.02	0.0020	5.1	1.2
2.2	0.117	573.78	0.0010	3.9	0.7
2.4	0.119	573.63	0.0005	2.8	0.35
2.6	0.120	573.52	0.0003	2	0.2
2.8	0.120	573.41	0.0002	2	0.2
3	0.121	573.31	0.0001	2	0.2
3.4	0.121	573.19	0.0001	2	0.2
3.8	0.125	573	0.0001	2	0.2
4.2	0.130	573	0.0001	2	0.2
4.6	0.131	573	0.0001	2	0.2
5.0	0.127	573	0.0001	2	0.2
>7.0	0.100	573	0.0001	2	0.2

r/d	v (m/s)	T (K)	$\overline{T^2}$ (K ²)	k 10 ⁴ (m ² /s ²)	ϵ 10 ³ (m ² /s ³)
0	0.202	595.65	0.3611	5.9	2.5
0.1	0.195	595.4	0.3634	6.2	2.8
0.2	0.189	594.76	0.4215	6.8	3.3
0.3	0.182	593.83	0.4879	7.6	4.2
0.4	0.176	592.68	0.5338	8.5	5.3
0.5	0.169	591.38	0.5457	9.3	6.1
0.6	0.163	589.99	0.5240	9.7	6.9
0.7	0.157	588.56	0.4772	9.9	7.1
0.8	0.151	587.13	0.4163	9.8	6.9
0.9	0.146	585.72	0.3509	9.6	6.6
1	0.140	584.38	0.2877	9	5.8
1.1	0.136	583.1	0.2303	8.2	5
1.2	0.131	581.91	0.1803	7.3	3.9
1.3	0.127	580.82	0.1376	6.4	3.1
1.4	0.123	579.82	0.1022	5.5	2.2
1.5	0.120	578.92	0.0734	4.8	1.7
1.6	0.117	578.13	0.0509	3.9	1.1
1.8	0.112	576.81	0.0220	3.1	0.7
2	0.109	575.84	0.0090	2.5	0.4
2.2	0.107	575.14	0.0043	2	0.3
2.4	0.106	574.65	0.0020	2	0.2
2.6	0.106	574.32	0.0002	2	0.2
2.8	0.106	574.09	0.0002	2	0.2
3	0.106	573.92	0.0001	2	0.2
3.4	0.107	573.67	0.0001	2	0.2
3.8	0.107	573.48	0.0001	2	0.2
4.2	0.109	573.37	0.0001	2	0.2
4.6	0.113	573.36	0.0001	2	0.2
5	0.116	573.25	0.0001	2	0.2
>7	0.100	573	0.0001	2	0.2